Bioactive Materials 6 (2021) 4542–4557

Contents lists available at ScienceDirect

Bioactive Materials

journal homepage: www.sciencedirect.com/journal/bioactive-materials

Practical strategy to construct anti-osteosarcoma bone substitutes by loading cisplatin into 3D-printed titanium alloy implants using a thermosensitive hydrogel

Zehao Jing [a,b,c], Renhua Ni [a,b], Jiedong Wang [a,b,c], Xinhong Lin [a,b,c], Daoyang Fan [a,b,c], Qingguang Wei [a,b,c], Teng Zhang [a,b,c], Yufeng Zheng [d,***], Hong Cai [a,b,**], Zhongjun Liu [a,b,c,*]

[a] Department of Orthopedics, Peking University Third Hospital, Beijing, 100191, People's Republic of China
[b] Engineering Research Center of Bone and Joint Precision Medicine, Ministry of Education, Beijing, 100191, People's Republic of China
[c] Beijing Key Laboratory of Spinal Disease Research, Beijing, 100191, People's Republic of China
[d] Department of Materials Science and Engineering, College of Engineering, Peking University, Beijing, 100871, People's Republic of China

ARTICLE INFO

Keywords:
3D-printed titanium alloy
Orthopaedic implant
Osteosarcoma
Hydrogel
Local chemotherapy

ABSTRACT

Surgical resection and perioperative adjuvant chemotherapy-based therapies have improved the prognosis of patients with osteosarcoma; however, intraoperative bone defects, local tumour recurrence, and chemotherapy-induced adverse effects still affect the quality of life of patients. Emerging 3D-printed titanium alloy (Ti_6Al_4V) implants have advantages over traditional implants in bone repair, including lower elastic modulus, lower stiffness, better bone conduction, more bone in-growth, stronger mechanical interlocking, and lager drug-loading capacity by their inherent porous structure. Here, cisplatin, a clinical first-line anti-osteosarcoma drug, was loaded into Ti_6Al_4V implants, within a PLGA-PEG-PLGA thermo-sensitive hydrogel, to construct bone substitutes with both anti-osteosarcoma and bone-repair functions. The optimal concentrations of cisplatin (0.8 and 1.6 mg/mL) were first determined *in vitro*. Thereafter, the anti-tumour effect and biosafety of the cisplatin/hydrogel-loaded implants, as well as their bone-repair potential were evaluated *in vivo* in tumour-bearing mouse, and bone defect rabbit models, respectively. The loading of cisplatin reduced tumour volume by more than two-thirds (from 641.1 to 201.4 mm^3) with negligible organ damage, achieving better anti-tumour effects while avoiding the adverse effects of systemic cisplatin delivery. Although bone repair was hindered by cisplatin loading at 4 weeks, no difference was observed at 8 weeks in the context of implants with versus without cisplatin, indicating acceptable long-term stability of all implants (with 8.48%–10.04% bone in-growth and 16.94%–20.53% osseointegration). Overall, cisplatin/hydrogel-loaded 3D-printed Ti_6Al_4V implants are safe and effective for treating osteosarcoma-caused bone defects, and should be considered for clinical use.

1. Introduction

Osteosarcoma is the most common primary malignant bone tumour in children and adolescents [1]. Surgical removal combined with pre- and post-operative neoadjuvant chemotherapy has become the standard procedure for the treatment of osteosarcoma [2]. However, bone defects are inevitably created during surgical interventions [3]. Additionally, due to the complex peri-tumour anatomy, it is not always practical to thoroughly excise the whole tumour for preventing tumour recurrence [4]. Although improvements in systemic adjuvant chemotherapy in recent years has substantially increased the long-term survival of patients to 60%–70%, more than 30% of patients eventually succumb to recurrence after surgery [5]. This may be due to the following intrinsic drawbacks of traditional chemotherapy administered intravenously. i) The untargeted therapeutics can cause serious systemic adverse effects, which limit the maximal dosage of therapeutics for the treatment of

Peer review under responsibility of KeAi Communications Co., Ltd.
* Corresponding author. Department of Orthopedics, Peking University Third Hospital, Beijing 100191, People's Republic of China.
** Corresponding author. Department of Orthopedics, Peking University Third Hospital, Beijing 100191, People's Republic of China.
*** Corresponding author. Department of Materials Science and Engineering, College of Engineering, Peking University, Beijing, 100871, People's Republic of China.
E-mail addresses: yfzheng@pku.edu.cn (Y. Zheng), hongcai@bjmu.edu.cn (H. Cai), zjliu@bjmu.edu.cn (Z. Liu).

https://doi.org/10.1016/j.bioactmat.2021.05.007
Received 13 February 2021; Received in revised form 12 April 2021; Accepted 3 May 2021

patients [6]. ii) The local drug concentration in the tumour site may not be high enough, as the organs deplete the drug from the blood, decreasing its concentration, and the operation destroys the local blood supply. It has been reported that, many times, the drug concentration in the postoperative area is too low to kill all tumour cells [7]. Importantly, these limitations can be overcome via local chemotherapy; such interventions deliver higher drug concentrations into the tumour microenvironment, while simultaneously avoiding severe systemic adverse effects [8,9]. Therefore, the generation of functional implants for both bone substitution and chemotherapeutic drug release is essential to further improve the treatment of patients with osteosarcoma.

Titanium alloys are the most commonly used materials for the generation of bone substitutes owing to their excellent biocompatibility, strength-to-weight ratio, and corrosion resistance [10]. However, the stiffness of traditional titanium alloy implants is considerably higher than that of cortical bone. An effective approach for reducing the biomechanical mismatch between titanium alloy implants and cortical bone is to fabricate porous structures, which cannot be achieved by conventional forging or casting techniques [11]. Therefore, additive manufacturing, also known as 3D printing, must be used for the fabrication of the desired shapes [12]. Currently, using 3D printing technologies based on electron beam melting (EBM) or selective laser sintering (SLM), porous Ti_6Al_4V implants can be printed by design and used in the orthopaedic clinical practice conveniently [13–21]. Importantly, compared with traditional titanium alloy implants, 3D-printed porous Ti_6Al_4V implants have significantly reduced elastic modulus and stiffness, similar to those of cortical bone and are therefore more suitable bone substitutes [22]. Of note, preclinical [23–26] and clinical [27–30] trials have confirmed the advantages of the porous structure of 3D-printed Ti_6Al_4V implants for bone defect repair over traditional titanium alloy implants, including better bone conduction, more bone in-growth, and stronger mechanical interlocking.

Importantly, the inherent higher surface area and interconnected pores make 3D-printed Ti_6Al_4V implants good drug carriers for local administration [31]. In our previous studies, simvastatin [32], recombinant human BMP-2 (rhBMP-2) [33], vascular endothelial growth factor (VEGF) [34], and vancomycin [35] were effectively loaded into 3D-printed porous Ti_6Al_4V implants, leading to an effective *in situ* drug release, better osseointegration and bone in-growth, and anti-infection effects as observed both *in vitro* and *in vivo* [32–35]. However, few antineoplastic 3D-printed Ti_6Al_4V implants have been tested *in vivo* [31].

Cisplatin is one of the most widely used anti-tumour agents and is usually administered intravenously for the treatment of osteosarcoma [36,37]. However, there are several problems associated with its intravenous administration, including nephrotoxicity, myelosuppression, nausea, emesis, and low drug concentration at the cancerous site(s). Local chemotherapy via intraperitoneal [38], transarterial [39], and intratumoural [8] administration has been performed clinically to address these problems. However, as low-molecular-weight chemotherapeutic drugs such as cisplatin rapidly pass into the blood circulation (their retention period in the tumour is very short), no significantly enhanced and prolonged anti-tumour effects have been reported [9].

PLGA-PEG-PLGA hydrogels are nontoxic biodegradable hydrogels based on poly(D,L-lactide-*co*-glycolide)-poly (ethylene glycol)-poly(D,L-lactide-*co*-glycolide) triblock copolymers [40,41]. Owing to the hydrophilic PEG and hydrophobic PLGA structures, the PLGA-PEG-PLGA hydrogels can incorporate both hydrophilic and hydrophobic drugs [42,43]. Furthermore, when the temperature changes from below to above the phase transition, hydrogels can be transformed from a sol-like state into a gelatinous state, making them suitable for drug loading *in vitro* and sustained drug release *in vivo* [44,45]. Although several other vehicles, including collagen, nanoparticles, and other hydrogels have been used in localised cisplatin or other chemotherapeutic drug delivery [7–9], the PLGA-PEG-PLGA thermosensitive hydrogel has numerous advantages, such as cheaper than collagen, larger in capacity than nanoparticles, and more accessible than most other hydrogels; commercialised PLAG-PEG-PLGA hydrogels have been widely sold. Therefore, the PLGA-PEG-PLGA hydrogels are promising scaffolds for local cisplatin delivery. However, owing to their poor mechanical properties, hydrogels cannot be used alone to repair bone defects; other materials should be used in conjunction [32]. For instance, the pores of 3D-printed Ti_6Al_4V implants can be filled with drug-loaded hydrogels for the generation of materials that can increase the concentration of drugs at the target sites [32].

In the present study, 3D-printed porous Ti_6Al_4V implants were fabricated and loaded with cisplatin using a PLGA-PEG-PLGA hydrogel as the vehicle. The anti-tumour effect and biosafety of the cisplatin/hydrogel-loaded implants were evaluated in the context of osteosarcoma *in vitro* and *in vivo*. Because of the potential cytotoxicity of chemotherapeutic agents on osteoblasts, the adverse effects of the drug-loaded implants on osteogenesis, bone in-growth, osseointegration, and bone-implant fixation were also evaluated *in vitro* and *in vivo* (Scheme 1).

2. Materials and methods

2.1. Fabrication of 3D-printed Ti_6Al_4V implants

3D-printed Ti_6Al_4V implants with porous structures (Fig. S1A in Supporting Information, Ø5 mm × L6 mm, pore size of 640 μm, and strut diameter of 400 μm) were fabricated using an EBM S12 system (Arcam AB, Molndal, Sweden) as previously described [34]. A cylindrical 3D model was designed, converted into a standard triangulation language (STL) file, and transferred to an EBM machine. Thereafter, medical-grade Ti_6Al_4V powder (particle size 45–100 μm) was melted layer by layer according to the STL data, and it was solidified by cooling. All samples were ultrasonically cleaned successively in acetone, ethyl alcohol, and deionised water (15 min each).

2.2. Preparation of cisplatin/hydrogel-loaded 3D-printed Ti_6Al_4V implants

The hydrogel was prepared as previously described [44,45]. PLGA (1500–2000)-PEG (1000–1500)-PLGA (1500–2000) thermosensitive hydrogel (Shanghai Yuanye Bio-Technology Co., Ltd., Shanghai, China) was added to deionised water while stirring; the polymer to water mass ratio was 1:4. After incubation for 7 nights at 4 °C, the gel completely dissolved and formed a clear viscous solution (Fig. S1D in Supporting Information). The gel was then loaded with a specific amount of cisplatin (Shanghai Yuanye Bio-Technology Co., Ltd.) (Fig. S1E in Supporting Information). The 3D-printed titanium alloy implants were placed inside a gel chamber, and equal volumes of cisplatin/hydrogel were injected into the pores at 4 °C (Fig. S1B in Supporting Information). The samples were warmed to room temperature (18–25 °C) before implantation to form the cisplatin/hydrogel-loaded 3D-printed Ti_6Al_4V implants (Figs. S1C and F in Supporting Information). The materials and components of the different complexes are listed in Table 1.

2.3. Characterisation of the cisplatin/hydrogel-loaded 3D-printed titanium alloy implants

2.3.1. Physical parameters

The physical parameters of the 3D-printed Ti_6Al_4V implants were determined using the following methods. The true density was measured using a helium gas pycnometer (AccuPyc 1330 Gas Pycnometer; Micromeritics Instruments, Norcross, GA, USA) [46]. The specific surface area was calculated using the Brunauer-Emmett-Teller method with krypton (the Kr-BET method), as reported elsewhere [47]. The porosity was analysed using a mercury porosimeter (PoreMasterGT 60, Quantachrome Instruments, Boynton Beach, FL, USA) [48], and the mechanical strength was determined using a mechanical testing system

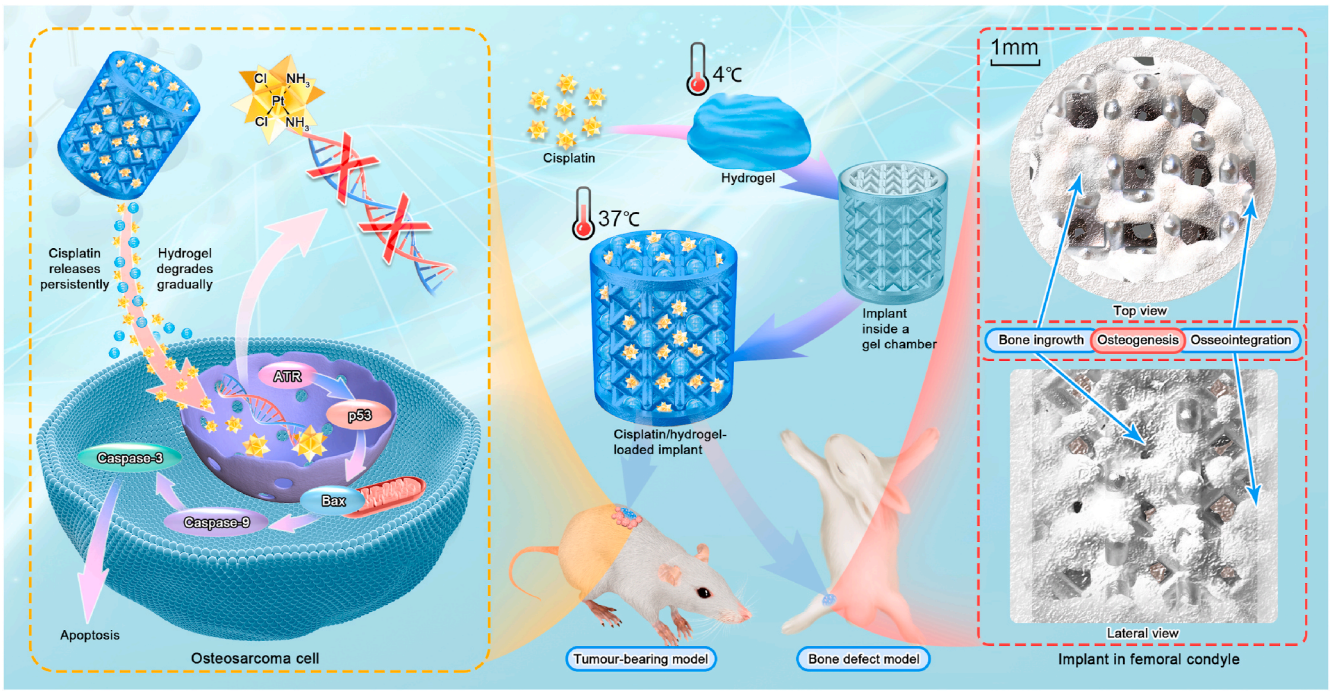

Scheme 1. Schematic illustration of the construction of cisplatin/hydrogel-loaded 3D-printed Ti_6Al_4V implants with anti-tumour and bone-repair effects.

Table 1
Cisplatin/hydrogel-loaded 3D-printed Ti_6Al_4V implants: the materials and their components.

Material	Component (w/w)
Cisplatin	Pt (purity: 65%)
PLGA-PEG-PLGA hydrogel	PLGA-PEG-PLGA (20.0%), Deionised water (80.0%)
3D-printed titanium alloy implants	Ti (90.0%), Al (5.7%), V (3.8%)

(Landmark, MTS Inc., Eden Prairie, MN, USA). Compression tests were performed at an initial strain rate of 10^{-3} s^{-1} at room temperature [49]. Samples were measured in triplicate.

2.3.2. Microstructure and composition

To determine the changes in the microstructure and composition of the 3D-printed Ti_6Al_4V implants before and after hydrogel/cisplatin loading, scanning electron microscopy (SEM), and energy dispersive spectroscopy (EDS) were performed. In detail, all samples were first freeze-dried at −50 °C and 1.5 mtorr/1.95 × 10^3 mbar for 3 days in a vacuum freeze drier (ModulyoD-230; Thermo Fischer Scientific, Waltham, MA, USA). Thereafter, SEM (S–3000 N, Hitachi, Japan) was used to determine the surface morphology; EDS was attached to the SEM apparatus and used to characterise the chemical composition [50].

2.3.3. Hydrogel degradation

To characterise the process of hydrogel degradation, 0.8 and 1.6 mg/mL cisplatin/hydrogel-containing implants (10 for each concentration) were placed in two glass bottles separately and immersed in 250 mL of PBS (pH 5.5) at 37 °C to imitate the postsurgical acidic conditions and extracellular microenvironment of tumour cells [51]. Of note, five of the cisplatin/hydrogel-containing implants at each concentration were stained in green with calcein to improve visualisation and photographed using a laser scanning confocal microscope every 3 days [32]. The other five implants at each concentration were weighed accurately at the same time. The mass of the remaining hydrogel is equal to the mass of hydrogel-containing implant at each time point minus that of implant without hydrogel. The percentage of mass remaining over time was calculated. Samples were measured in triplicate.

2.3.4. Cisplatin release

To determine the *in vitro* release kinetics of cisplatin incorporated in PLAG-PEG-PLAG hydrogel-loaded 3D-printed Ti_6Al_4V implants, modified drug release experiments were performed [51]. Briefly, 0.8 and 1.6 mg/mL cisplatin/hydrogel-containing implants (10 for each concentration) were placed in two glass bottles separately and immersed in 250 mL of PBS (pH 5.5) at 37 °C. At predetermined time points, 5.0 mL of extracting solution was collected from each bottle, and the bottles were refilled with equal volumes of PBS (pH 5.5). The concentration of platinum in each extracting solution was determined using an inductively coupled plasma mass spectrometer (ICP-MS, Xseries II; Thermo Fischer Scientific, Waltham, MA, USA) to reflect the amount of released cisplatin [52]. The percentage of cisplatin released over time was calculated. Samples were measured in triplicate.

2.4. In vitro anti-tumour effect and biosafety

To test the anti-tumour effect of the cisplatin/hydrogel-loaded 3D-printed Ti_6Al_4V implants *in vitro*, osteosarcoma (143B, HOS, and MG63) cells were co-cultured with the complexes and cell viability was determined using Cell Counting Kit-8 (CCK-8; Dojindo, Kumamoto, Japan). In brief, the cells were seeded in 48-well plates (15,000 cells per well in 600 mL of DMEM containing 10% foetal bovine serum, 50 U/mL penicillin, and 50 U/mL streptomycin), and incubated at 37 °C under a 5% CO_2 atmosphere for 24 h. The complexes with cisplatin at concentrations of 0, 0.01, 0.1, 1, and 10 mg/mL were then added to the wells, and the samples were incubated for 24, 48, or 72 h. The culture medium was then replaced with DMEM. Finally, cell viability was calculated using CCK-8 according to the manufacturer's instructions; the optical density was measured using a microplate reader (Varioskan Flash; Thermo Fisher Scientific, Waltham, MA, USA) at a wavelength of 450 nm.

To further detect the optimal cisplatin concentration in hydrogel-loaded 3D-printed Ti_6Al_4V implants, complexes with different concentrations of cisplatin (0, 0.4, 0.8, 1.2, 1.6, and 2.0 mg/mL) were co-

cultured with osteosarcoma (143B, HOS, and MG63) cells and primary human osteoblasts (HUM-iCell-s021, Shanghai iCELL Bio-technology Co., Ltd., Shanghai, China) [53] for 48 h. Co-cultures and cell viability detection were performed as described above.

2.5. In vivo anti-tumour effect and biosafety

2.5.1. Tumour-bearing nude mouse model

The anti-tumour effect and biosafety of the cisplatin/hydrogel-loaded 3D-printed Ti_6Al_4V implants were evaluated *in vivo* using 5-week-old female BALB/c nude mice. The Peking University Institutional Review Board on Biomedical Ethics in the Care and Use of Laboratory Animals approved all animal experiment protocols (Project Number: LA2020465). The mice (13–17 g) were subcutaneously injected with 0.2 mL of cell suspension containing 1.0×10^7 human osteosarcoma 143B cells in PBS into the right scapula. Grouping and treatments were started after 1 week, when the volume of the tumours reached ~100 mm^3.

2.5.2. Grouping

The mice were weighed and randomly divided into five groups (five mice per group). Each mouse then received an implant, placed subcutaneously, adjacent to the tumour. Implants without hydrogel and cisplatin were used in the control group (implant group). Cisplatin (0, 0.8, and 1.6 mg/mL)/hydrogel-loaded implants were used in three different experimental groups (implant + hydrogel group, implant + hydrogel + cisplatin 0.8 mg/mL group, and implant + hydrogel + cisplatin 1.6 mg/mL group). Additionally, a positive control group was also established via the systemic delivery of cisplatin (3 μg of cisplatin per gram of mice body weight through tail intravenous injection twice a week) together with the use of hydrogel-free implants (implant + systemic cisplatin delivery group).

2.5.3. Tumour volume and body weight

The anti-tumour effect and biosafety were assessed *in vivo* by measuring the tumour volume and body weights twice a week for up to 17 days. The tumour volume was calculated using the following equation:

$$V = L \times W^2 \times 0.5,$$

where, L (mm) and W (mm) are the largest and smallest diameters of the tumour mass, respectively [54].

2.5.4. Tumour weight and organ index

After treatment, all mice were sacrificed. The tumour masses and organs, including the heart, liver, spleen, lungs, and kidneys of each mouse were weighed immediately. Organ indices were calculated using the following equation [55]:

$$\text{Organ index} = \text{organ weight}/\text{body weight} \times 100.$$

2.5.5. Blood tests

On day 17 after surgery, tail tip blood and whole blood from the ophthalmic vein were collected from the mice before euthanasia; serum was also obtained after blood coagulation. Blood glucose level was measured using a blood glucose meter (ACCU-CHEK; Roche Diabetes Care GmbH, Mannheim, Germany) after starving the mice for 12 h. All blood routine tests, including the determination of white blood cell count (WBC), haemoglobin (Hb) level, red blood cell count (RBC), haematocrit (HCT), mean corpuscular haemoglobin concentration (MCHC), mean corpuscular haemoglobin (MCH) level, mean corpuscular volume (MCV), red blood cell distribution width coefficient of variation (RDW-CV), platelet count (PLT), mean platelet volume (MPV), platelet distribution width (PDW), and platelet haematocrit (PCT), were performed using an automatic blood cell analyser (MEK-7222K; NIHON KOHDEN CORP., Japan). Additionally, biochemical parameters, including aspartate aminotransferase (AST), alanine aminotransferase (ALT), creatine kinase (CK), blood urea nitrogen (BUN), and serum creatinine (Scr), were measured using an automatic biochemical analyser (AU480 Chemistry Analyser; Beckman Coulter, Brea, CA, USA).

2.5.6. H&E staining

For histological staining, the tumours, heart, liver, spleen, lung, and kidney of the sacrificed mice were collected and fixed in 4% (w/v) paraformaldehyde. The tissue sections were stained with haematoxylin and eosin (H&E) for histological analysis to evaluate tumour pathology and organ damage.

2.5.7. TUNEL assay

The terminal nucleotidyltransferase-mediated nick end labelling (TUNEL) assay was performed according to the manufacturer's protocol (Roche, Basel, Switzerland). Briefly, the nicked DNA ends of the tissue sections were labelled with the reaction mixture. Cell apoptosis was observed by fluorescence microscopy.

2.5.8. Immunohistochemistry

Immunohistochemistry (IHC) was performed to detect proteins within the tumours. Briefly, tumour tissue specimens were cut into 10-μm sections after dewaxing and hydration. The soaked sections were placed in 3% H_2O_2-methanol to block endogenous peroxidase activity. The sections were then incubated with normal goat serum for 10 min and incubated with *anti*-ATR/p53/Bax/Caspase-9/Caspase-3 antibodies (dilution 1:200) at 4 °C overnight. The next day, the sections were washed with PBS and incubated with biotinylated secondary antibodies at 37 °C for 45 min. The sections were washed again with PBS and incubated with horseradish peroxidase-labelled streptavidin at 37 °C. The samples were developed with diaminobenzidine (DAB) and stained with haematoxylin. After normal washing, dehydration, lucidification, and mounting, the sections were observed under a microscope. The integrated optical density (IOD) was measured, to accurately reflect total protein expression. Positive IHC areas were analysed using Image-Pro Plus 6.0 software.

2.6. In vivo osteogenesis

2.6.1. Bone defect rabbit model and grouping

The Peking University Institutional Review Board on Biomedical Ethics in the Care and Use of Laboratory Animals approved all animal experimental protocols (Project Number: LA2020465). Forty adult female New Zealand white rabbits (25 weeks, 3.5 ± 0.3 kg) were randomly assigned into four groups (five rabbits per group) and subjected to surgery to create bone defects. The surgical procedures were performed with the rabbits under general anaesthesia using pentobarbital sodium (30 mg kg^{-1}, i.p.), as previously described [56]. Briefly, the left and right lateral femoral condyles were exposed, and cylindrical defects of diameter 5 mm and depth 6 mm were drilled. Implants without hydrogel and cisplatin were inserted into the predrilled defects in the control group (implant group). Additionally, cisplatin (0, 0.8 and 1.6 mg/mL)/hydrogel-loaded implants were used in the three experimental groups (implant + hydrogel group, implant + hydrogel + cisplatin 0.8 mg/mL group, and implant + hydrogel + cisplatin 1.6 mg/mL group).

2.6.2. Sampling

Four weeks after surgery, 20 randomly selected rabbits were euthanised (five rabbits from each group). All sacrificed rabbits (with five left and five right femur specimens from each group) were prepared for micro-CT analyses. The left femurs (five specimens in each group) were then cut into undecalcified histological slices, and the right femurs (five specimens in each group) were prepared for mechanical push-out tests. The remaining 20 animals were euthanised 8 weeks after surgery, and the same scheme as above was used.

2.6.3. Micro-CT analysis

Ten specimens (including five left and five right femur specimens) from each group were scanned by micro-CT (Siemens, Munich, Germany) at a scanning rate of 6°/min and a resolution of 9 μm. The X-ray source voltage was 80 kV, and the beam current was 80 mA using filtered Bremsstrahlung radiation. A 1-mm aluminium filter was used during the scanning. The micro-CT images were then reconstructed using multimodal 3D visualisation software (Inveon Research Workplace; Siemens, Munich, Germany). The bone was distinguished from soft tissue and titanium implants by partitioning different Hounsfield units (HUs). The phase of the bone was defined in the range of 1000–2250 HU. After the reconstruction, the peripheral 500-μm region around and the intra-porous space within the implant were selected as the region of interest (ROI). In the ROI, the bone volume/tissue volume (BV/TV, the ratio of bone volume to total volume) and trabecular separation (Tb.Sp, mean width of the medullary cavity between bone trabeculae) were calculated using Inveon Research Workplace software (Siemens, Munich, Germany).

2.6.4. Undecalcified bone histology

Undecalcified bone sections were prepared for bone in-growth and osseointegration analyses, as previously described [57]. Briefly, five left femur specimens in each group were fixed in 10% formalin for 14 days and dehydrated in serial concentrations of ethanol (40%, 75%, 95%, and 100%) for 3 days each. The specimens were then embedded in methyl methacrylate and sectioned using a powered saw with diamond blade of the EXAKT system (EXAKT Apparatebau, Norderstedt, Germany). The ground sections of 40–50 μm were then prepared using the system and finally subjected to Masson Goldner's trichrome staining (bone tissues are stained green, osteoid tissues are stained red/orange, and the implants appear black). The entire stained sections were photographed using NanoZoomer (Hamamatsu Photonics, Hamamatsu, Japan), and then observed under an optical microscope (Olympus BH-2; Olympus America Inc., USA). Quantitative analysis was performed using Image-Pro Plus software (version 6.0) with two middle longitudinal sections of each block for both bone in-growth and osseointegration determination [57]. Thus, 10 slices were analysed for each group at each time point. Bone in-growth was defined as the percentage of new bone within the pores. The amount of bone in-growth was equal to the area of bone over the area of pores. Osseointegration was measured as a fraction of the surface area of the implant in contact with the bone. The tissue sections were viewed at a high magnification to accurately calculate the circumference of the implant and the length of the bone-covered implant. The length of the implant covered by bone divided by the circumference of the implant was the value of osseointegration.

2.6.5. Push-out test

A mechanical testing system (Landmark; MTS Inc., Eden Prairie, MN, USA) was used to measure the push-out force between the implant and bone, as previously described [57]. Briefly, five right femur specimens in each group were carefully cut at a tangent angle to the long axis of the implant to expose the inner side of the implant, and the periosteal bone at the outer side was removed before testing. A custom-designed special holder was applied to fix the sample to ensure loading alignment, and then, the push-out procedure was carried out at a constant rate of 1.5 mm/min. The endpoint of the test was the presence of an abrupt drop in the push-out force, and the maximal load was recorded as the push-out force.

2.7. Statistical analysis

Data are presented as mean ± standard deviation (SD). Statistical analysis was performed using SPSS 12.0 software. A one-way analysis of variance (ANOVA) followed by Tukey's post hoc test was used in experiments with more than two groups, and a two-way *t*-test was used in experiments with two groups at each time point. Statistical significance was set at $P < 0.05$.

3. Results and discussion

3.1. Characterisation of the cisplatin/hydrogel-loaded 3D-printed Ti_6Al_4V implants

To comprehensively characterise the developed 3D-printed Ti_6Al_4V implants, their structural and physical characteristics (true density, specific surface area, porosity, and nominal stress) were determined using various methods. As listed in Table 2, the physical characteristics of the newly fabricated 3D-printed Ti_6Al_4V implants in this study are similar to those reported previously [32], and support their suitability for bone substitution and drug loading [32–35].

To confirm the presence of cisplatin and hydrogel in the pores of 3D-printed Ti_6Al_4V implants, bare, hydrogel-loaded, and cisplatin/hydrogel-loaded implants were analysed by SEM and EDS. As shown in Fig. S2A in the Supporting Information and Fig. 1A, SEM revealed that the bare implants showed a highly aligned porous structure; importantly, the cross-linked hydrogels, as well as the incorporated cisplatin particles, were observed by SEM in the pores of the hydrogel-loaded and cisplatin/hydrogel-loaded implants, respectively, implying that cisplatin can be loaded into the pores of the implants within the hydrogel. Additionally, the EDS results clarified the inherent elements of the Ti_6Al_4V implants (titanium, aluminium, and vanadium) and the increase in the carbon (C) and oxygen (O) content in hydrogel-loaded implants (Fig. S2B in the Supporting Information). Moreover, a similar distribution of the representative elements of cisplatin (Pt) and hydrogel (C and O) were detected by EDS layered images (Fig. 1B), further confirming the ability of the hydrogel to incorporate cisplatin into the pores of the Ti_6Al_4V implants.

Next, the rate of hydrogel degradation within the 3D-printed Ti_6Al_4V implants was profiled *in vitro*. Laser scanning confocal microscopy (Fig. 1C) and the calculation of the remaining mass (Fig. 1D) demonstrated that the hydrogel remains in the pores of the implants for at least 15 days. The release kinetics of cisplatin *in vitro* was also evaluated via the detection of the concentration of platinum in a solution mimicking extracellular acidic microenvironment of tumour cells (Fig. 1E). Interestingly, although there was an initial burst release, the process of cisplatin release was sustained for more than 15 days *in vitro*, regardless of the amount of drug loaded into the hydrogel (Fig. 1E).

To our knowledge, this is the first report on the degradation and cisplatin release behaviour of PLGA-PEG-PLGA hydrogels in 3D-printed porous titanium alloy implants. Compared with the finding of Ma et al., that is, the PLGA-PEG-PLGA hydrogels (20 wt%) degraded over 40 days *in vitro* [44], the hydrogels in this study degraded faster, a phenomenon that may be attributed to the acidity of the extracting solution and the larger contact area between the hydrogels and the extracting solution in the scaffold. The release period of cisplatin coincided with the degradation period of the hydrogel, implying that the release of cisplatin was dependent on the degradation of hydrogel, which was consistent with the results of EDS layered images (Fig. 1B, cisplatin was incorporated by hydrogels and then loaded into the scaffolds, and was not freely present on the implant surface).

In the meantime, an interesting phenomenon was observed, that is, a small portion of the swollen hydrogel dropped off the scaffold when immersed in the solution, showing a reduction in the weight of the

Table 2
Characteristics of the 3D-printed Ti_6Al_4V implants.

Characteristic	Method	Value
True density	Gas displacement technique	4.4103 ± 0.0042 g/cm
Specific surface area	Kr-BET method	0.00408 ± 0.00063 m^2/g
Porosity	Mercury porosimeter	69.0% ± 0.11%
Nominal stress	Mechanical testing system	58.0 ± 18.1 MPa

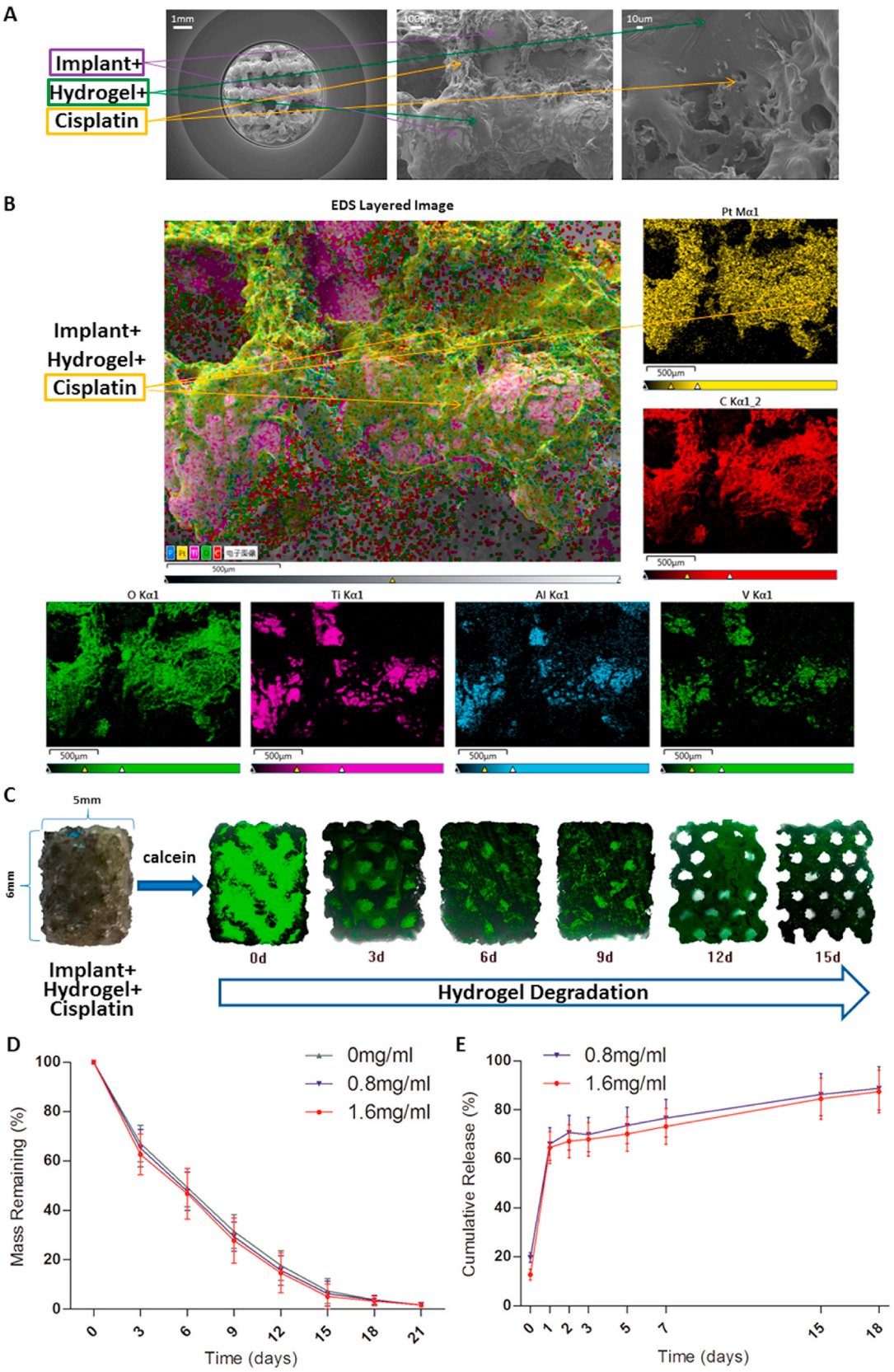

Fig. 1. Characterisation of the cisplatin/hydrogel-loaded 3D-printed Ti_6Al_4V implants. (A) Representative SEM images of the implants. The cross-linked hydrogels and the incorporated cisplatin particles can be seen in the images. (B) Representative EDS layered images of the implants. Various elements are coloured. The distribution of platinum is the same as those of carbon and oxygen but different from those of titanium, aluminium, and vanadium, suggesting that cisplatin was incorporated in the hydrogel. Degradation of the hydrogel loaded in the implants *in vitro*: (C) degradation and (D) mass remaining (n = 3). The transparent hydrogel was stained with calcein (green) to improve visualisation. (E) The release profile of cisplatin from the implants *in vitro* (n = 3).

hydrogel on the scaffold and no release of cisplatin. This resulted in a decrease in the remaining hydrogel mass faster than the increase in cisplatin cumulative release. Consequently, the mass remaining of the hydrogel on the scaffold at 15 days was less than 10% (Fig. 1D), but approximately 20% of cisplatin was not released at the same time (Fig. 1E).

3.2. *In vitro* anti-tumour effect and biosafety of the cisplatin/hydrogel-loaded 3D-printed Ti_6Al_4V implants

As both the anti-tumour effect and biosafety are dependent on the drug concentration, the appropriate concentration range of cisplatin in the hydrogel-loaded implants should balance the therapeutic action and adverse effects. Therefore, the implants loaded with hydrogel and cisplatin at multiple concentrations (0, 0.01, 0.1, 1.0, and 10 mg/mL for the first round test and 0, 0.4, 0.8, 1.2, 1.6, and 2.0 mg/mL for the

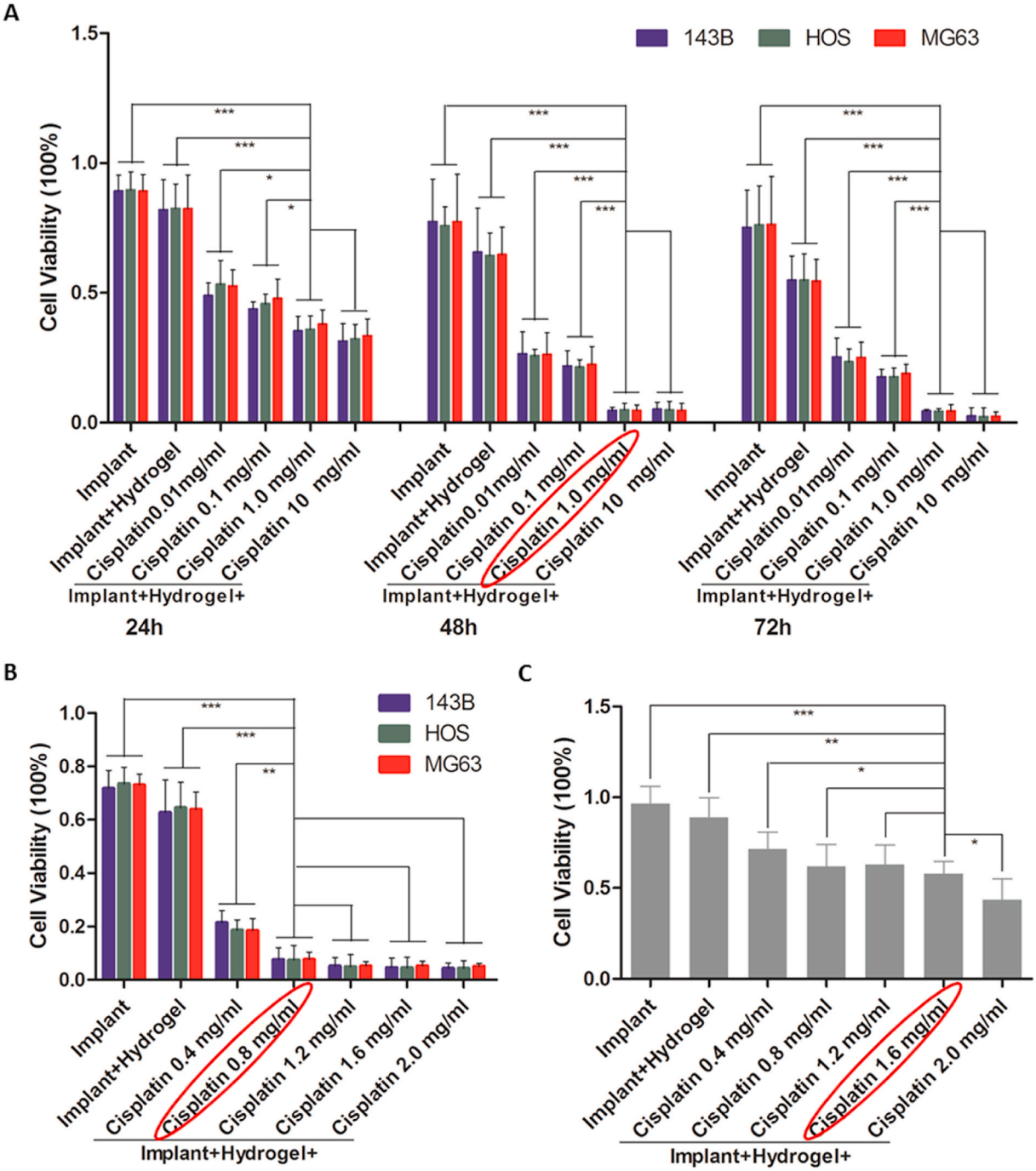

Fig. 2. *In vitro* anti-tumour effect and biosafety of the cisplatin/hydrogel-loaded 3D-printed Ti_6Al_4V implants. (A) The viability of osteosarcoma cells (143B, HOS, and MG63) after incubation with bare implants, hydrogel-loaded implants, and 0.01, 0.1, 1.0, 10 mg/mL cisplatin/hydrogel-loaded implants for 24, 48, and 72 h. (B) The viability of osteosarcoma cells (143B, HOS, and MG63) after incubation with bare implants, hydrogel-loaded implants, and 0.4, 0.8, 1.2, 1.6, 2.0 mg/mL cisplatin/hydrogel-loaded implants for 48 h. (C) The viability of primary human osteoblasts after incubation with bare implants, hydrogel-loaded implants, and 0.4, 0.8, 1.2, 1.6, 2.0 mg/mL cisplatin/hydrogel-loaded implants for 48 h. Data are represented as mean ± standard deviation (n = 6). *p < 0.05, **p < 0.01, ***p < 0.001.

second round test) were co-cultured with osteosarcoma (143B, HOS, and MG63) cells and primary human osteoblasts. Although the *in vitro* experiment could not fully reflect the situation *in vivo*, as the previous drug concentrations could not be used as a reference in the new set of experiments, the dose of cisplatin screened in the *in vitro* experiment was used as an important reference for the *in vivo* experiment in this study. As shown in Fig. 2, the cisplatin/hydrogel-loaded 3D-printed Ti_6Al_4V implants reduced the viability of osteosarcoma cells and osteoblasts in a dose- and time-dependent manner. In the first round of testing, 1.0 mg/mL was selected as the reference concentration for the next round of testing, because at this concentration, the complex was sufficient to kill more than 90% of osteosarcoma cells (Fig. 2A). In the next round of testing, implants loaded with cisplatin at 0.8–1.6 mg/mL killed more than 90% of osteosarcoma cells after co-culture for 48 h (Fig. 2B), while killing less than 50% of osteoblasts (Fig. 2C). Therefore, 0.8 and 1.6 mg/mL were selected as the reference doses for animal experiments.

The scaffold on top of a cell monolayer may damage the cells. However, the uneven undersides of the scaffold had limited contact with the underlying cells, and therefore, it did not greatly affect the results. For a scaffold loaded with hydrogel, the hydrogel at the bottom of the scaffold also touched the cells, which may be one of the reasons that the addition of hydrogel reduced cell viabilities. However, the area of this contact was also limited, because the area of the bottom of a 48-well plate is approximately four times that of the titanium alloy implant.

3.3. *In vivo* anti-tumour effect and biosafety of the cisplatin/hydrogel-loaded 3D-printed Ti_6Al_4V implants

The *in vivo* anti-tumour effect and biosafety of the cisplatin/hydrogel-loaded 3D-printed Ti_6Al_4V implants were investigated in a human osteosarcoma xenograft model induced via the subcutaneous inoculation of human osteosarcoma 143B cells into the right scapula of nude mice. When the volume of the tumours reached ~100 mm^3, the mice were treated with different implants (peritumoural treatment).

As shown in Fig. 3A, the tumour volumes increased rapidly in the animals treated with bare implants (implant group), or implants loaded with hydrogel only (implant + hydrogel group). In contrast, the animals treated with implants loaded with hydrogel and cisplatin (implant + hydrogel + cisplatin 0.8 mg/mL and 1.6 mg/mL groups) displayed a dose-dependent anti-tumour effect (Fig. 3A), with the significant suppression of tumour growth (Fig. 3A) and mild inhibition of body weight gain (Fig. 3B) compared with those in the implant group. Importantly, these results suggest that drug loading is an effective and safe method for the treatment of osteosarcoma, which is in line with previous studies [7,44]. Of note, although the systemic administration of cisplatin (implant + systemic cisplatin delivery group) significantly reduced the tumour volume (Fig. 3A), the anti-tumour effect was not better than that observed in the implant + hydrogel + cisplatin 0.8 mg/mL group and was worse than that observed in the implant + hydrogel + cisplatin 1.6 mg/mL group. Moreover, systemic drug delivery significantly decreased the body weight of nude mice (compared with the weight of mice in the other groups; Fig. 3B), suggesting the occurrence of obvious adverse effects. Although there have been several studies on local drug delivery [7,44], few have directly compared local drug delivery with systemic drug delivery [8]. To our knowledge, this study is the first to demonstrate that the implantation of cisplatin/hydrogel-loaded implants for the local administration of cisplatin has significant advantages over the traditional systemic cisplatin delivery in terms of both anti-tumour effects and biosafety.

At the experiment endpoint, the osteosarcoma tumour masses and organs including the heart, liver, spleen, lungs, and kidneys were dissected and weighed; the organ indices were then calculated. Of note, the results of tumour masses (Fig. S3A in the Supporting Information) were consistent with those of tumour volumes, showing that 1.6 mg/mL cisplatin/hydrogel-loaded implants had the best anti-tumour effect among all groups, and 0.8 mg/mL cisplatin/hydrogel-loaded implants and systemic cisplatin delivery had similar anti-tumour effects. Interestingly, as shown in Figs. S3B–F in the Supporting Information, there were no significant differences in the heart (Fig. S3B in the Supporting Information) and lung (Fig. S3E in the Supporting Information) indices among all groups, whereas the systemic cisplatin delivery significantly decreased the liver (Fig. S3C in the Supporting Information) and spleen (Fig. S3D in the Supporting Information) indices and increased the kidney index (Fig. S3F in the Supporting Information) as expected compared with those in the other groups. These results further confirm the toxicity of systemic cisplatin delivery and the biosafety of local cisplatin administration.

Blood tests were also performed to investigate the biosafety of the cisplatin/hydrogel-loaded implants. Overall, most of the indicators were comparable among the groups (Table S1 in the Supporting Information), except WBC, PLT, PCT, AST, BUN, and BUN/Scr showing significant differences among the groups (Fig. 3C–H). Of note, while the results demonstrated that the implantation of 1.6 mg/mL cisplatin/hydrogel-loaded implants affected the blood cellular and biochemical profiles, the effects were milder than those observed with systemic cisplatin delivery. Importantly, reducing the amount of cisplatin to 0.8 mg/mL could avoid the effect on the blood (reflected by the WBC, PLT, and PCT measurements) and on hepatorenal functions (reflected by the AST, BUN, and BUN/Scr measurements).

Next, the tumour masses were cut into sections for the pathology analysis. As shown in Fig. 4A, numerous tumour cells with increased nuclear size and different shapes were observed in the tumour masses treated with bare implants or hydrogel-loaded implants. In contrast, karyolysis (dissolution of cell nucleus), pyknosis (condensation of chromatin), and karyorrhexis (fragmentation of nucleus) [44] were clearly observed in the tumours treated with cisplatin/hydrogel-loaded implants as well as via systemic cisplatin delivery, indicating obvious tumour necrosis. Furthermore, TUNEL staining revealed that the group treated with 1.6 mg/mL cisplatin/hydrogel-loaded implants exhibited the highest fluorescence among all groups (Fig. 4A), implying the highest rate of apoptotic tumour cells (Fig. S4A in the Supporting Information). Contrarily, few apoptotic cells were observed in the implant group and implant + hydrogel group (Fig. 4A), indicating that apoptosis was cisplatin dependent.

ATR/p53/Bax/Caspase-9/Caspase-3 is a classical signalling pathway in cisplatin-induced cell apoptosis [58–60]. Within cells, cisplatin forms covalent bonds with the purine bases in the DNA, resulting in intra-strand cross-linking, and the consequent double-strand breaks and blocking of DNA replication and gene transcription [61,62]. The consequent genotoxic stress results in the recruitment of ATR, a molecular sensor of DNA damage, and the successive activation of p53, Bax, and caspase superfamily proteins for the induction of apoptosis [58]. Therefore, we investigated the anti-tumour mechanism of the cisplatin complexes via the evaluation of ATR, p53, Bax, Caspase-9, and Caspase-3 expression in osteosarcoma tumour masses from different groups by IHC. As shown in Fig. 4B, compared with tumours from animals treated with bare implants or hydrogel-loaded implants, the expression of apoptosis-related proteins significantly increased in the tumours from animals treated with cisplatin/hydrogel-loaded implants and systemic cisplatin delivery. This was clearly observed when the expression data were quantified. As shown in Figs. S4B–F in the Supporting Information, tumours from the implant + hydrogel + cisplatin 1.6 mg/mL group expressed the most apoptosis proteins, followed closely by those from the implant + hydrogel + cisplatin 0.8 mg/mL group and from the implant + systemic cisplatin delivery group. Overall, these data suggest, as expected, that apoptosis was induced by the activation of the ATR/p53/Bax/Caspase-9/Caspase-3 pathway in a cisplatin-dependent manner, consistent with the results of TUNEL staining (Figs. 4A and S4A in the Supporting Information).

Finally, systemic toxicity was evaluated via the morphological analysis of H&E-stained heart, liver, kidney, lung, and spleen tissue sections (Fig. S4G in the Supporting Information). In agreement with the

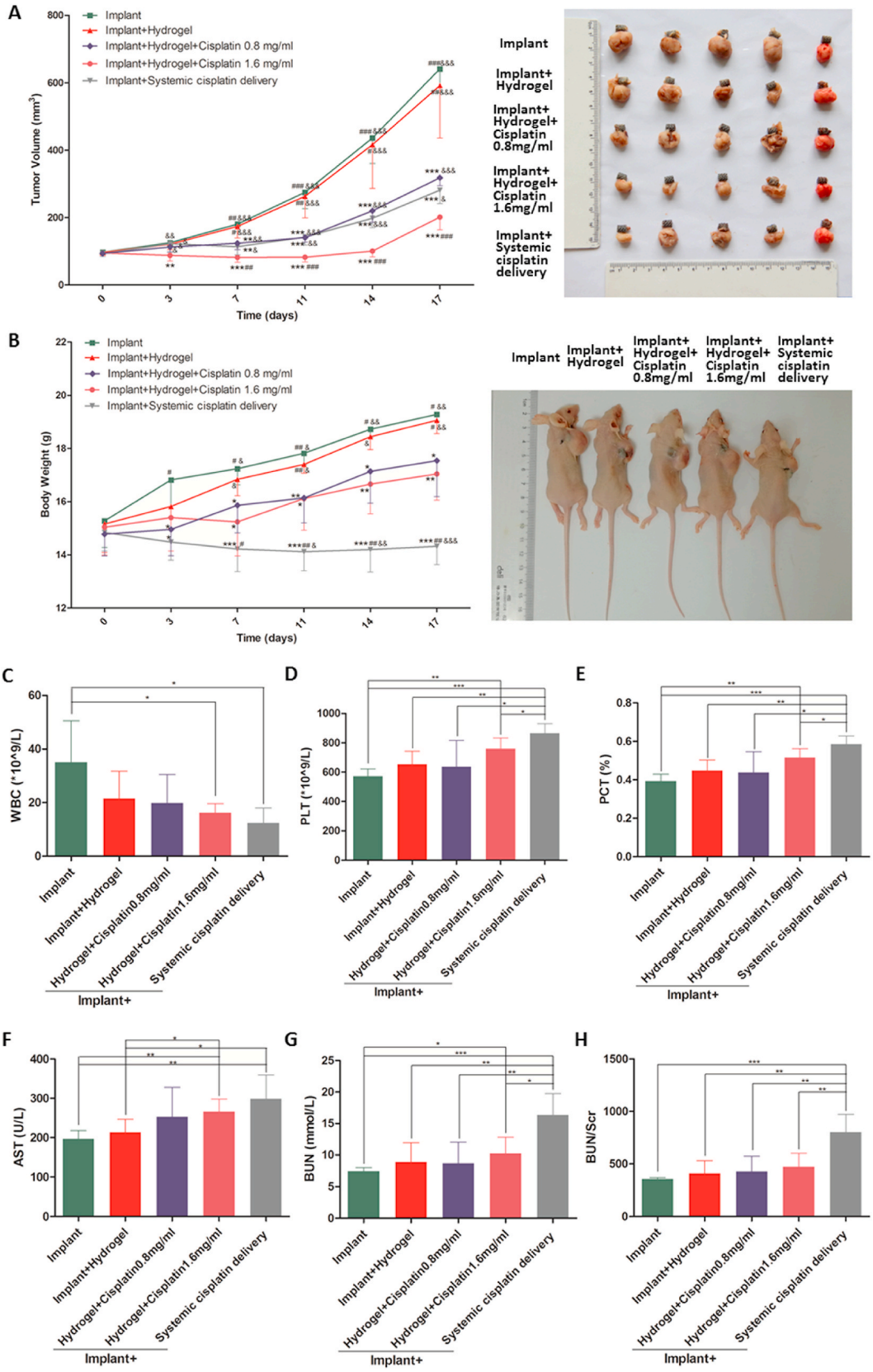

Fig. 3. *In vivo* anti-tumour effect and biosafety of the cisplatin/hydrogel-loaded 3D-printed Ti_6Al_4V implants. Human osteosarcoma 143B cells were inoculated subcutaneously into BALB/c nude mice; tumour progression was monitored. The tumour volume (A) and body weight of mice (B) were measured twice a week throughout the experiment. The blood routine and biochemical parameters (C–H) were determined immediately after sacrificing the mice. Systemic cisplatin delivery via tail intravenous injection of 3 μg of cisplatin per gram of mice body weight twice a week. Data are represented as mean ± standard deviation (n = 5). (A–B) *p < 0.05, **p < 0.01, ***p < 0.001 compared with the implant group; #p < 0.05, ##p < 0.01, ###p < 0.001 compared with the implant + hydrogel + cisplatin 0.8 mg/mL group; &p < 0.05, &&p < 0.01, &&&p < 0.001 compared with the implant + hydrogel + cisplatin 1.6 mg/mL group. (C–H) *p < 0.05, **p < 0.01, ***p < 0.001.

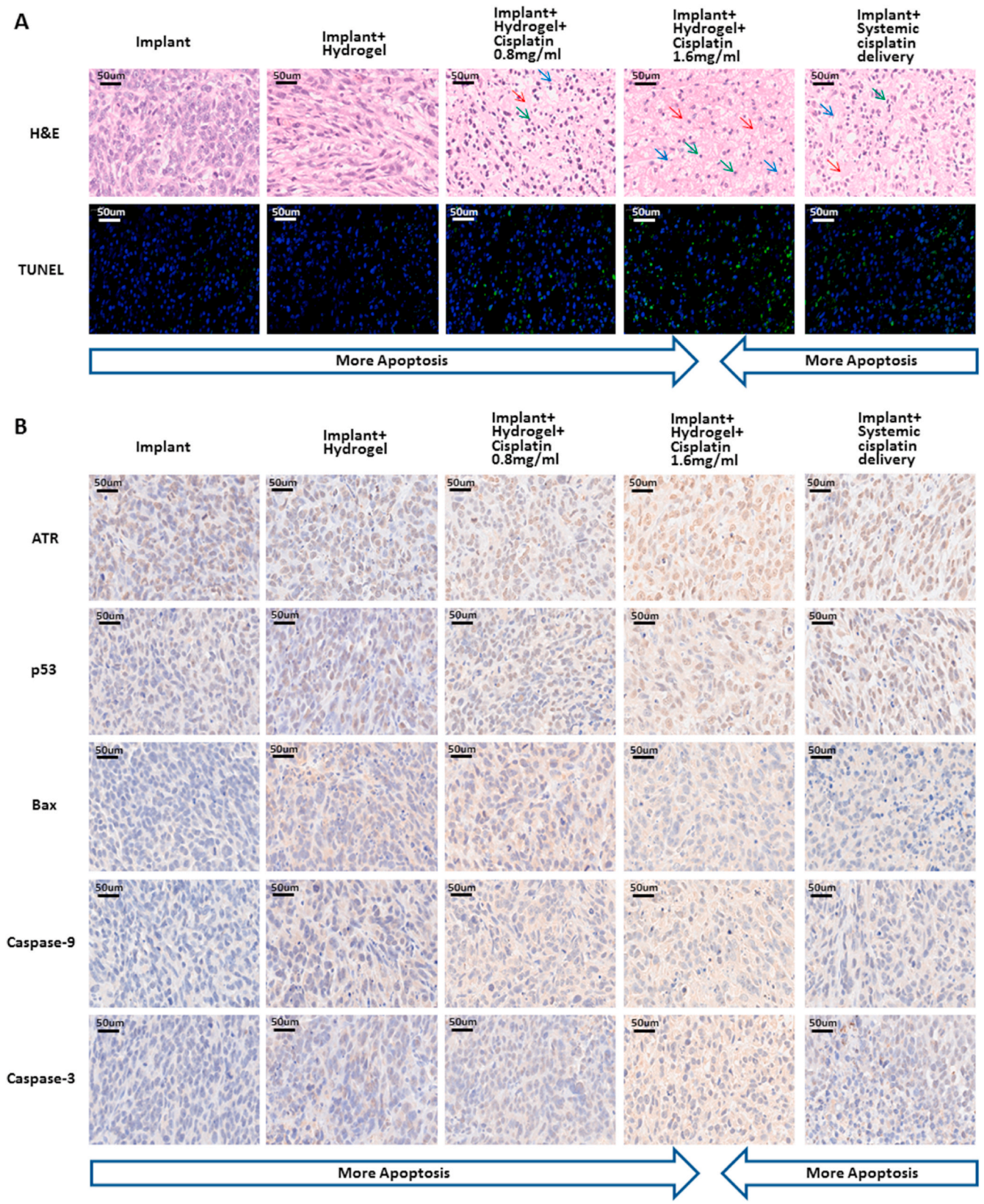

Fig. 4. Anti-tumour effect and biosafety of the cisplatin/hydrogel-loaded 3D-printed Ti_6Al_4V implants: histology and immunohistochemistry findings of the *in vivo* study. (A) Representative H&E staining and TUNEL assay of tumour sections under various treatments. Nuclei are stained blue (red arrow for karyolysis, green arrow for pyknosis, and blue arrow for karyorrhexis); the extracellular matrix and the cytoplasm are stained red. Green fluorescence indicates apoptotic cells in the TUNEL analysis. (B) Representative immunohistochemistry images of tumour sections from mice subjected to various treatments: ATR, p53, Bax, Caspase-9, and Caspase-3. Scale bars = 50 μm.

findings of previous studies [63,64], swelling of renal tubules, which could be a reason for the increased kidney index (Fig. S3F in the Supporting Information), was observed in animals treated systemically with cisplatin, indicating renal toxicity (Fig. S4G in the Supporting Information). On the contrary, there were no abnormalities in the organs of mice from any other group (Fig. S4G in the Supporting Information), implying no obvious organotoxicity of the cisplatin/hydrogel-loaded implants. This may be attributed to the fact that the peritumoural implantation of drug-loaded implants led to the localised and sustained release of chemotherapeutics, and therefore, had a relatively low

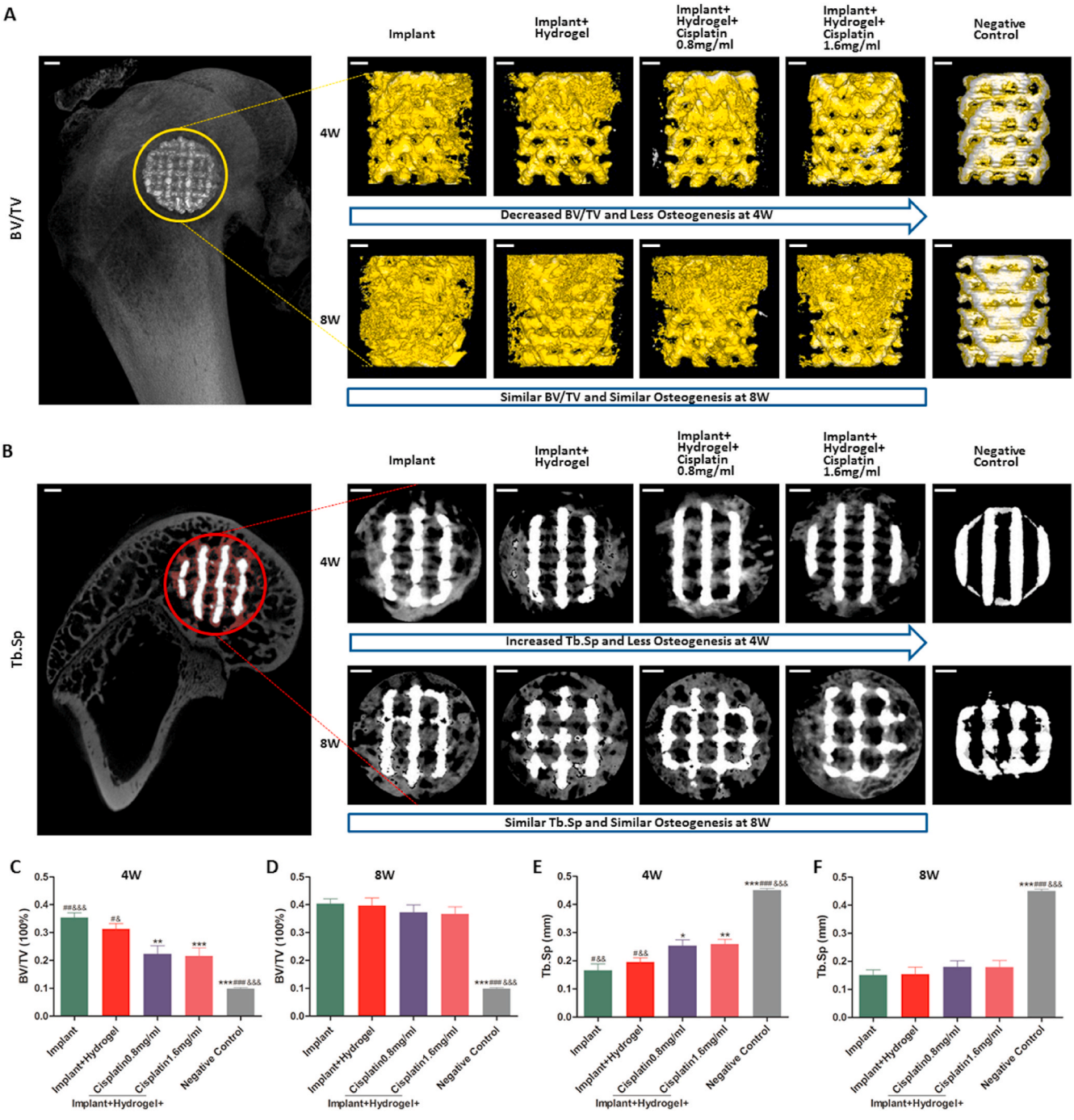

Fig. 5. *In vivo* osteogenic potential of the cisplatin/hydrogel-loaded 3D-printed Ti_6Al_4V implants. A bone defect rabbit model (femoral condyle defect) was used. Briefly, critical bone defects were surgically generated and filled with different implants. After 4 and 8 weeks, the peripheral 500-μm region around and the intraporous space within the implants were reconstructed (A), sectioned (B), and analysed (C) by micro-CT. In the representative reconstruction images (A), the bone and the implants are labelled in yellow and silver, respectively; the bone volume/tissue volumes (BV/TV, the ratio of bone volume to total volume) are intuitively reflected by the amount of bone on the implants (yellow in the pictures). In the representative sectioned images (B), the bone and the implants are labelled in grey and white, respectively; the trabecular separations (Tb.Sp, mean width of the medullary cavity between bone trabeculae) are intuitively reflected by the amount of interspace in the bone (black in the grey). The quantitative results of osteogenesis, including the BV/TV (C and D) and Tb.Sp (E and F), in the various groups, are shown. Data are represented as mean ± standard deviation (n = 10). *p < 0.05, **p < 0.01, ***p < 0.001 compared with the implant group; #p < 0.05, ##p < 0.01, ###p < 0.001 compared with the implant + hydrogel + cisplatin 0.8 mg/mL group; &p < 0.05, &&p < 0.01, &&&p < 0.001 compared with the implant + hydrogel + cisplatin 1.6 mg/mL group. Scale bars = 1 mm.

systemic effect [44].

3.4. Effect of cisplatin/hydrogel-loaded 3D-printed Ti_6Al_4V implants on osteogenesis, bone in-growth, and osseointegration in vivo

A widely accepted bone defect model in rabbits (femoral condyle defect, Figs. S5A–B in the Supporting Information) was used to evaluate the bone repair effect of the implants [57]. Femur specimens were harvested 4 and 8 weeks after surgery for micro-CT analysis, undecalcified histology, and push-out tests to evaluate osteogenesis, bone in-growth, and osseointegration in and around the implants.

Osteogenesis was analysed by micro-computed tomography (micro-CT). The implant and the bone in the ROIs of all femur specimens were reconstructed (Fig. 5A) and sectioned (Fig. 5B). Two indicators (BV/TV, positively associated with osteogenesis, and Tb.Sp, negatively associated with osteogenesis) were calculated (Fig. 5C–F). Of note, as we found that micro-CT inevitably mistook metal artefacts for new bone, a negative control was set up using an implant that was scanned and reconstructed immediately after implantation, to eliminate the interference of metal artefacts and verify the accuracy of the data obtained. As shown in Fig. 5, the BV/TV (~10%) and Tb.Sp (~45%) of the negative control were substantially different from those in the other groups, indicating that the accurate calculation of these two indicators by micro-CT analysis was possible, although with a small margin of error. Moreover, referring to similar studies published previously, in which BV/TV was ~26.7% at 4 weeks and ~29% at 8 weeks [32,57], we found that the results of BV/TV in the implant group (~35% at 4 weeks and ~40% at 8 weeks) were within a reasonable range considering the artefact-induced ~10% increase; this comparison further validates the measurement method used in this study.

Interestingly, as illustrated in Fig. 5, the BV/TV grew over time, and, conversely, the Tb.Sp decreased, indicating that more osteogenesis, and no bone resorption occurred from weeks 4–8; these results are consistent with those previously reported by us, with the same implants [32]. Of note, at 4 weeks, the BV/TV significantly decreased with the loading of cisplatin into the implants (Fig. 5A and C), whereas the Tb.Sp significantly increased simultaneously (Fig. 5B and E); conversely, there was no difference between the implant group and implant + hydrogel group in terms of BV/TV and Tb.Sp at 4 weeks (Fig. 5A–C and E). However, at 8 weeks, the BV/TV and Tb.Sp showed no differences among all groups (Fig. 5A–B, D and F). Overall, these results suggest that although the local administration of cisplatin decreases osteogenesis early (4 weeks) after implantation, it does not affect long-term (8 weeks) osteogenesis.

Additionally, bone in-growth and osseointegration were evaluated via undecalcified histology (Figs. 6 and S6 in the Supporting Information); specimens were subjected to Masson Goldner's trichrome staining to distinguish the mineralised bone tissues (bone stained in green; Fig. 6A–B and S6 in the Supporting Information). Of note, these two indicators in the implant group reached ~10% and ~20%, respectively, at 8 weeks, in line with the results reported previously [57].

Importantly, consistent with the results of osteogenesis (Fig. 5A–C and E), at 4 weeks, the bone in-growth and osseointegration significantly decreased after the implantation of cisplatin-loaded versus bare implants, alone, or together with hydrogel alone (Fig. 6A and C-D). On the contrary, there was no difference among all groups at 8 weeks (Fig. 6B and E-F), which was also in agreement with the results of osteogenesis (Fig. 5A–B, D and F). Thus, these results further confirm that cisplatin in the 3D-printed Ti_6Al_4V implants impair bone in-growth and osseointegration early (4 weeks), but not later (8 weeks), after transplantation.

Of note, the comparison of the results of bone in-growth and osseointegration at different time points revealed that, from weeks 4–8, osseointegration significantly increased (Fig. 6A–B, D and F) but bone in-growth did not (Fig. 6A–B, C and E). This may be because the bone in-growth of 3D-printed porous Ti_6Al_4V implants reaches its peak at approximately 4 weeks; thereafter, the absorption and in-growth of bone achieves a dynamic equilibrium to complete the bone remodelling process [65]. Therefore, we hypothesise that while the bone mass in the pores remained unchanged, the bone contact with the implant (osseointegration) increased.

3.5. Impact of cisplatin/hydrogel-loaded 3D-printed Ti_6Al_4V implants on the fixation strength

Bone implant fixation is the epitome of osteogenesis, bone in-growth, and osseointegration; thus, the fixation strength of the implants using the right femur specimens was evaluated via push-out tests using a mechanical testing system (Fig. S7 in the Supporting Information). The typical displacement curves (Fig. 7A) and push-out forces (Fig. 7B–C) of the 3D-printed Ti_6Al_4V implants at weeks 4 and 8 after implantation were recorded. At week 4, cisplatin-loaded implants showed flatter displacement curves (Fig. 7A) and lower push-out forces (Fig. 7B) than those in the context of cisplatin-loaded implants, indicating that the cisplatin-loaded implants required a lower force to generate a similar displacement and reach the maximal force after short-term implantation. However, the differences in displacement curves (Fig. 7A) and push-out force (Figs. 7C and 0.3–0.4 kilonewtons, consistent with our previous study findings [57]) between cisplatin-loaded and bare implants (with or without hydrogel) disappeared 8 weeks after implantation, suggesting that the decrease in the fixation strength caused by cisplatin loading did not last long.

The possible mechanisms of the reduced osteogenesis, bone in-growth, osseointegration, and fixation strength at week 4 and their recovery at week 8 are worth discussing. Although the inhibitory effect of cisplatin systemic delivery on bone healing has been recognised [66], to our knowledge, this study is the first to demonstrate the same effect of localised cisplatin. We speculated that the inhibitory effect of localised cisplatin on bone healing was realised by increasing the level of inflammatory factors (such as tumour necrosis factor alpha) in the plasma on one hand, the same as cisplatin systemic delivery [66], and by direct killing of peripheral osteoblasts on the other hand (Fig. 2C). As cisplatin was fully released within week 4, both these factors disappeared from weeks 4–8, leading to compensatory osteogenesis around the implant, resulting in the recovery at week 8. However, this study does not directly confirm the effect of localised cisplatin on inflammatory factors in the plasma, although there are some indicators of blood testing that can be used as a reference (Fig. 3C–H), which is a limitation of this study.

4. Conclusions

In this study, a practical strategy was proposed to construct implants with anti-osteosarcoma and bone repair effects. Vehiculated within a PLGA-PEG-PLGA thermo-sensitive hydrogel, cisplatin can be conveniently loaded into 3D-printed Ti_6Al_4V implants. To the best of our knowledge, this is the first study to combine cisplatin with a 3D-printed titanium alloy implant via a thermosensitive hydrogel, in order to exploit the advantages of cisplatin in anti-osteosarcoma, hydrogel in drug sustained release, and metal scaffold in mechanical properties. Importantly, we demonstrate the cisplatin/hydrogel-loaded 3D-printed Ti_6Al_4V implants are safe and show a good anti-tumour potential both *in vitro* and *in vivo*. The results in the context of a tumour-bearing mouse model demonstrated that the implants had better anti-osteosarcoma effects and fewer adverse effects than the conventional systemic cisplatin delivery method, inducing higher tumour cell apoptosis, lower body weight loss, and little organ toxicity. Additionally, we show that although cisplatin loading decreases the bone repair effect of 3D-printed Ti_6Al_4V implants at 4 weeks after surgery, indicators including osteogenesis, bone in-growth, osseointegration, and bone-implant fixation strength fully recover at 8 weeks after implantation, indicating acceptable long-term stability.

In summary, our study proves that cisplatin/hydrogel-loaded 3D-printed titanium Ti_6Al_4V implants are practical and safe bone substitutes with excellent anti-osteosarcoma and acceptable bone repair

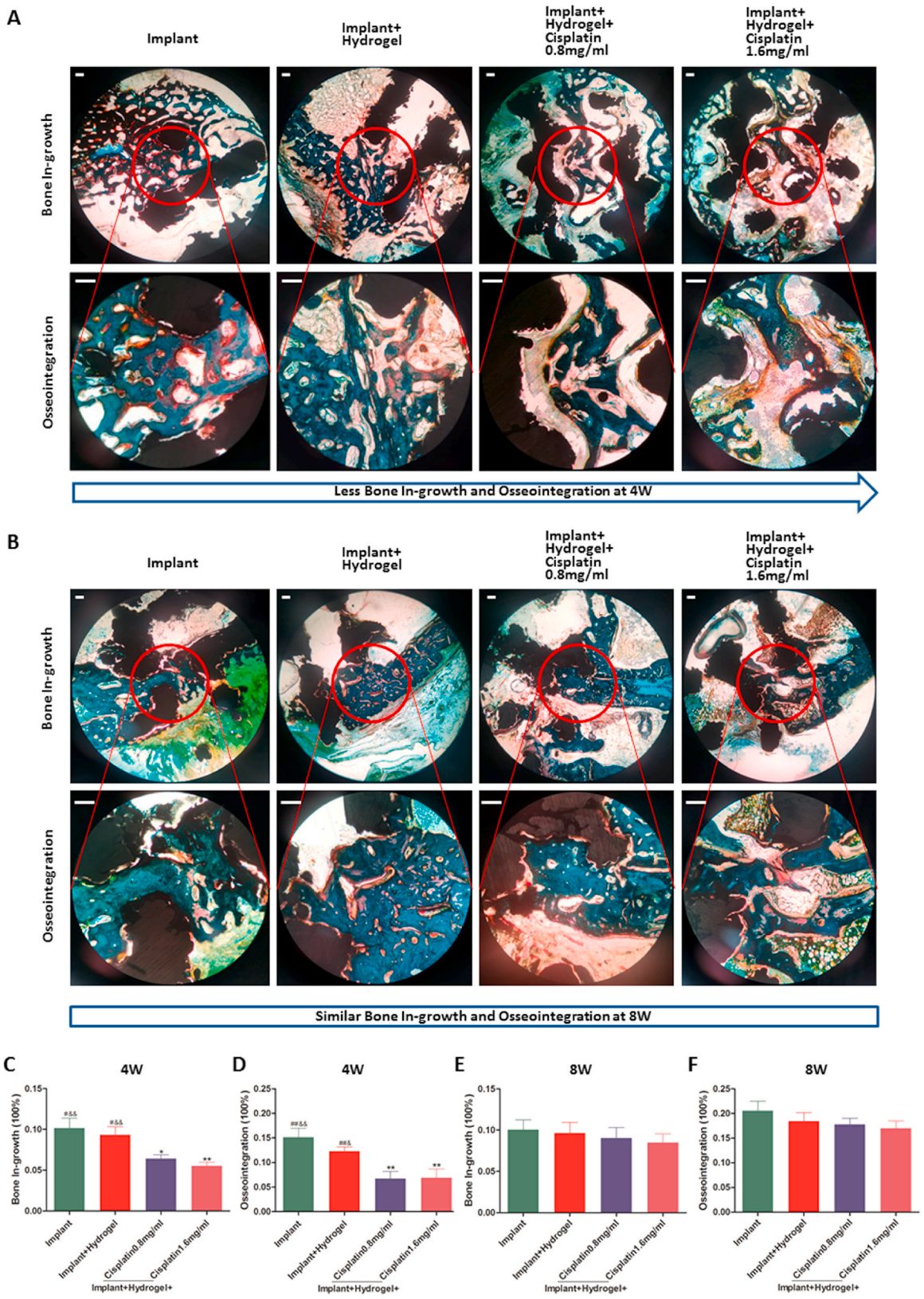

Fig. 6. Bone in-growth and osseointegration of the cisplatin/hydrogel-loaded 3D-printed Ti_6Al_4V implants *in vivo*. In the representative images of undecalcified histological sections stained with Masson Goldner's trichrome at 4 (A) and 8 (B) weeks after surgery, the mineralised bone tissues are stained green, the osteoid tissues are stained red/orange, and the implants appear black. The quantitative results of bone in-growth (C and E) and osseointegration (D and F) in the different groups were obtained using Image-Pro Plus 6.0 software based on two middle longitudinal sections. Data are represented as mean ± standard deviation (n = 10). *p < 0.05, **p < 0.01, ***p < 0.001 compared with the implant group; #p < 0.05, ##p < 0.01, ###p < 0.001 compared with the implant + hydrogel + cisplatin 0.8 mg/mL group; &p < 0.05, &&p < 0.01, &&&p < 0.001 compared with the implant + hydrogel + cisplatin 1.6 mg/mL group. Scale bars = 200 μm.

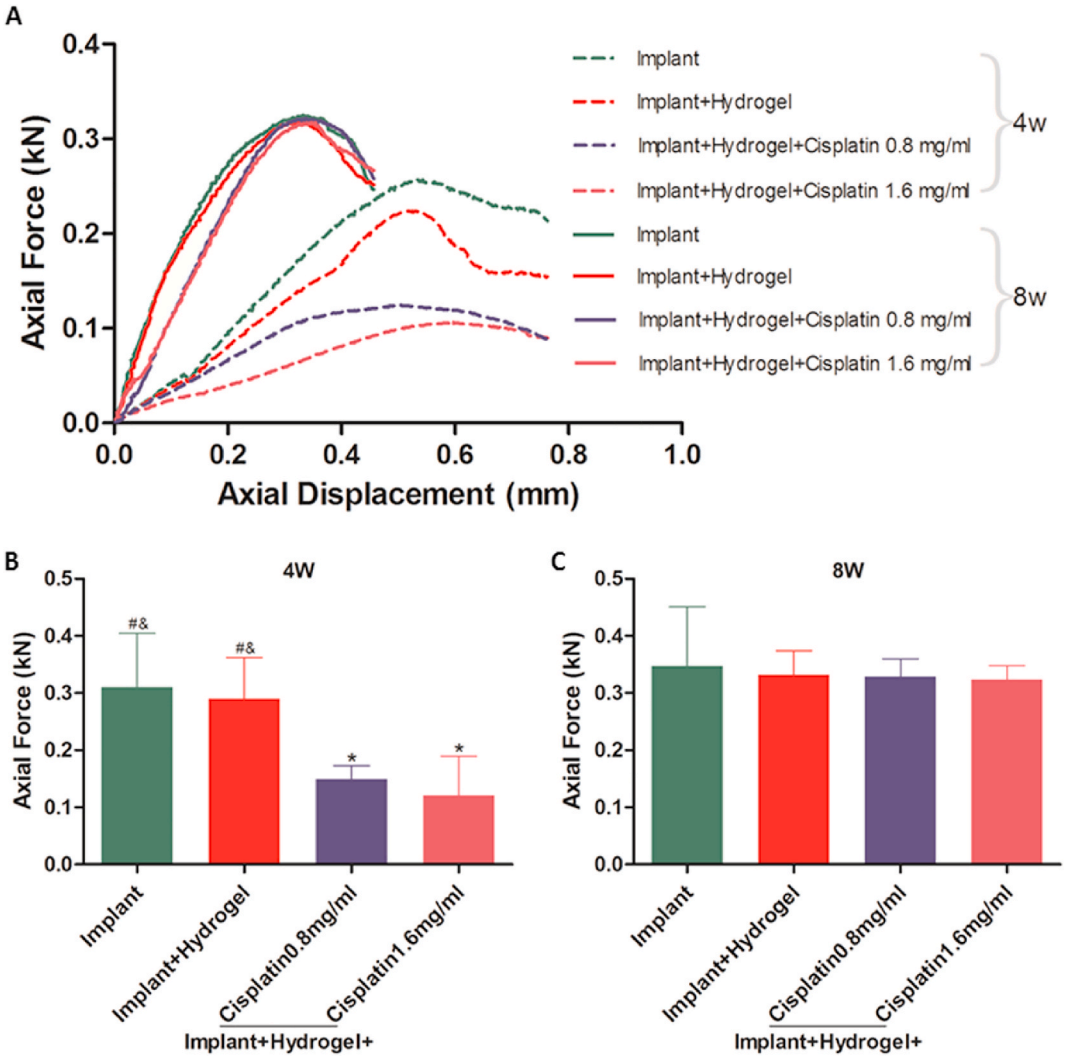

Fig. 7. Fixation strength of the cisplatin/hydrogel-loaded 3D-printed Ti_6Al_4V implants *in vivo*. Push-out tests were performed to obtain the typical displacement curves (A) and the push-out forces at weeks 4 (B) and 8 (C) to evaluate the fixation strengths. Data are represented as mean ± standard deviation (n = 5). *p < 0.05, **p < 0.01, ***p < 0.001 compared with the implant group; #p < 0.05, ##p < 0.01, ###p < 0.001 compared with the implant + hydrogel + cisplatin 0.8 mg/mL group; &p < 0.05, &&p < 0.01, &&&p < 0.001 compared with the implant + hydrogel + cisplatin 1.6 mg/mL group.

effects. As 3D-printed titanium alloys [13–21] and cisplatin [36,37] have been approved for clinical use, and the PLGA-PEG-PLGA hydrogel and its degradation products are non-toxic [40,41], this strategy has great potential for clinical translation.

CRediT authorship contribution statement

Zehao Jing: Methodology, Investigation, Writing – original draft, Visualization, Formal analysis, Data curation, Software. **Renhua Ni:** Methodology, Investigation, Writing – original draft, Visualization, Formal analysis, Data curation, Software. **Jiedong Wang:** Visualization, Formal analysis, Methodology. **Xinhong Lin:** Investigation, Data curation. **Daoyang Fan:** Methodology, Investigation. **Qingguang Wei:** Formal analysis, Writing – review & editing, Validation. **Teng Zhang:** Methodology, Writing – review & editing, Validation. **Yufeng Zheng:** Conceptualization, Writing – review & editing. **Hong Cai:** Conceptualization, Writing – review & editing, Resources. **Zhongjun Liu:** Conceptualization, Writing – review & editing, Supervision, Project administration, Funding acquisition.

Acknowledgements

Z.J. and R.N. contributed equally to this work. Z.L., H.C., and Y.Z. are the corresponding authors. The authors acknowledge the research support from the Beijing AKEC Medical Co., Ltd. and the guidance of Huijie Leng in biomechanics, Hong Wang in histology, Wanqiong Yuan in cell experiments, and Kuo Zhang in animal experiments.

Appendix A. Supplementary data

Supplementary data to this article can be found online at https://doi.org/10.1016/j.bioactmat.2021.05.007.

Funding

This work was supported by the Ministry of Science and Technology of the People's Republic of China [grant number 2016YFB1101501] and the National Natural Science Foundation of China [grant number 81772320].

Declaration of competing interest

None.

References

[1] E. Ward, C. DeSantis, A. Robbins, B. Kohler, A. Jemal, Childhood and adolescent cancer statistics, Ca-Cancer J. Clin. 64 (2) (2014) 83–103, https://doi.org/10.3322/caac.21219, 2014.

[2] M.S. Isakoff, S.S. Bielack, P. Meltzer, R. Gorlick, Osteosarcoma: current treatment and a collaborative pathway to success, J. Clin. Oncol. 33 (27) (2015) 3029–3035, https://doi.org/10.1200/JCO.2014.59.4895.

[3] F. Altaf, M. Weber, N. Dea, S. Boriani, C. Ames, R. Williams, J.J. Verlaan, I. Laufer, C.G. Fisher, Evidence-based review and survey of expert opinion of reconstruction of metastatic spine tumors, Spine 41 (Suppl 20) (2016) S254–S261, https://doi.org/10.1097/BRS.0000000000001819.

[4] N.A. Quraishi, A. Rajabian, A. Spencer, G. Arealis, H. Mehdian, B.M. Boszczyk, K. L. Edwards, Reoperation rates in the surgical treatment of spinal metastases, Spine J. 15 (3 Suppl) (2015) S37–S43, https://doi.org/10.1016/j.spinee.2015.01.005.

[5] F. Berrino, R. De Angelis, M. Sant, Survival for eight major cancers and all cancers combined for European adults diagnosed in 1995-99: results of the EUROCARE-4 study (vol 8, pg 773, 2007), Lancet Oncol. 8 (10) (2007), https://doi.org/10.1016/S1470-2045(07)70245-0, 868-868.

[6] K.A. Janeway, H.E. Grier, Sequelae of osteosarcoma medical therapy: a review of rare acute toxicities and late effects, Lancet Oncol. 11 (7) (2010) 670–678, https://doi.org/10.1016/S1470-2045(10)70062-0.

[7] M. Konishi, Y. Tabata, M. Kariya, A. Suzuki, M. Mandai, K. Nanbu, K. Takakura, S. Fujii, In vivo anti-tumor effect through the controlled release of cisplatin from biodegradable gelatin hydrogel, J. Contr. Release 92 (3) (2003) 301–313, https://doi.org/10.1016/S0168-3659(03)00364-X.

[8] K.A. Walter, R.J. Tamargo, A. Olivi, P.C. Burger, H. Brem, Intratumoral chemotherapy, Neurosurgery 37 (6) (1995) 1129–1145, https://doi.org/10.1227/00006123-199512000-00013.

[9] S.C. Ning, N. Yu, D.M. Brown, S. Kanekal, S.J. Knox, Radiosensitization by intratumoral administration of cisplatin in a sustained-release drug delivery system, Radiother. Oncol. 50 (2) (1999) 215–223, https://doi.org/10.1016/S0167-8140(98)00134-0.

[10] S.L. Mei, H.Y. Wang, W. Wang, L.P. Tong, H.B. Pan, C.S. Ruan, Q.L. Ma, M.Y. Liu, H.L. Yang, L. Zhang, Y.C. Cheng, Y.M. Zhang, L.Z. Zhao, P.K. Chu, Antibacterial effects and biocompatibility of titanium surfaces with graded silver incorporation in titania nanotubes, Biomaterials 35 (14) (2014) 4255–4265, https://doi.org/10.1016/j.biomaterials.2014.02.005.

[11] K.C. Nune, A. Kumar, L.E. Murr, R.D.K. Misra, Interplay between self-assembled structure of bone morphogenetic protein-2 (BMP-2) and osteoblast functions in three-dimensional titanium alloy scaffolds: stimulation of osteogenic activity, J. Biomed. Mater. Res. 104 (2) (2016) 517–532, https://doi.org/10.1002/jbm.a.35592.

[12] T.J. Snyder, M. Andrews, M. Weislogel, P. Moeck, J. Stone-Sundberg, D. Birkes, M. P. Hoffert, A. Lindeman, J. Morrill, O. Fercak, S. Friedman, J. Gunderson, A. Ha, J. McCollister, Y.K. Chen, J. Geile, A. Wollman, B. Attari, N. Botnen, V. Vuppuluri, J. Shim, W. Kaminsky, D. Adams, J. Graft, 3D Systems' technology overview and new applications in manufacturing, engineering, science, and education, 3d Print Addit, Man (Lond.) 1 (3) (2014) 169–176, https://doi.org/10.1089/3dp.2014.1502.

[13] A. Ataee, Y.C. Li, C.E. Wen, A comparative study on the nanoindentation behavior, wear resistance and in vitro biocompatibility of SLM manufactured CP-Ti and EBM manufactured Ti64 gyroid scaffolds, Acta Biomater. 97 (2019) 587–596, https://doi.org/10.1016/j.actbio.2019.08.008.

[14] B.J. Zhao, H. Wang, N. Qiao, C. Wang, M. Hu, Corrosion resistance characteristics of a Ti-6Al-4V alloy scaffold that is fabricated by electron beam melting and selective laser melting for implantation in vivo, Mat. Sci. Eng. C-Mater. 70 (2017) 832–841, https://doi.org/10.1016/j.msec.2016.07.045.

[15] H. Wang, B.J. Zhao, C.K. Liu, C. Wang, X.Y. Tan, M. Hu, A comparison of biocompatibility of a titanium alloy fabricated by electron beam melting and selective laser melting, PloS One 11 (7) (2016), e0158513, https://doi.org/10.1371/journal.pone.0158513.

[16] L. Li, J.P. Shi, K.J. Zhang, L.F. Yang, F. Yu, L.Y. Zhu, H.X. Liang, X.S. Wang, Q. Jiang, Early osteointegration evaluation of porous Ti6Al4V scaffolds designed based on triply periodic minimal surface models, J. Orthop. Transl. 19 (2019) 94–105, https://doi.org/10.1016/j.jot.2019.03.003.

[17] V.V. Popov, G. Muller-Kamskii, A. Kovalevsky, G. Dzhenzhera, E. Strokin, A. Kolomiets, J. Ramon, Design and 3D-printing of titanium bone implants: brief review of approach and clinical cases, Biomed. Eng. Lett. 8 (4) (2018) 337–344, https://doi.org/10.1007/s13534-018-0080-5.

[18] S.P. Narra, P.N. Mittwede, S.D. Wolf, K.L. Urish, Additive manufacturing in total joint arthroplasty, Orthop. Clin. N. Am. 50 (1) (2019) 13–20, https://doi.org/10.1016/j.ocl.2018.08.009.

[19] H. Wang, K.X. Su, L.Z. Su, P.P. Liang, P. Ji, C. Wang, Comparison of 3D-printed porous tantalum and titanium scaffolds on osteointegration and osteogenesis, Mat. Sci. Eng. C-Mater. 104 (2019), https://doi.org/10.1016/J.Msec.2019.109908.

[20] C.N. Kelly, N.T. Evans, C.W. Irvin, S.C. Chapman, K. Gall, D.L. Safranski, The effect of surface topography and porosity on the tensile fatigue of 3D printed Ti-6Al-4V fabricated by selective laser melting, Mat. Sci. Eng. C-Mater. 98 (2019) 726–736, https://doi.org/10.1016/j.msec.2019.01.024.

[21] W.F. Yang, W.S. Choi, Y.Y. Leung, J.P. Curtin, R.X. Du, C.Y. Zhang, X.S. Chen, Y. X. Su, Three-dimensional printing of patient-specific surgical plates in head and neck reconstruction: a prospective pilot study, Oral Oncol. 78 (2018) 31–36, https://doi.org/10.1016/j.oraloncology.2018.01.005.

[22] S.J. Li, Q.S. Xu, Z. Wang, W.T. Hou, Y.L. Hao, R. Yang, L.E. Murr, Influence of cell shape on mechanical properties of Ti-6Al-4V meshes fabricated by electron beam melting method, Acta Biomater. 10 (10) (2014) 4537–4547, https://doi.org/10.1016/j.actbio.2014.06.010.

[23] Q. Ran, W. Yang, Y. Hu, X. Shen, Y. Yu, Y. Xiang, K. Cai, Osteogenesis of 3D printed porous Ti6Al4V implants with different pore sizes, J. Mech. Behav. Biomed. Mater. 84 (2018) 1–11, https://doi.org/10.1016/j.jmbbm.2018.04.010.

[24] K.C. McGilvray, J. Easley, H.B. Seim, D. Regan, S.H. Berven, W.K. Hsu, T.E. Mroz, C.M. Puttlitz, Bony ingrowth potential of 3D-printed porous titanium alloy: a direct comparison of interbody cage materials in an in vivo ovine lumbar fusion model, Spine J. 18 (7) (2018) 1250–1260, https://doi.org/10.1016/j.spinee.2018.02.018.

[25] H. Wang, K.X. Su, L.Z. Su, P.P. Liang, P. Ji, C. Wang, The effect of 3D-printed Ti6Al4V scaffolds with various macropore structures on osteointegration and osteogenesis: a biomechanical evaluation, J. Mech. Behav. Biomed. Mater. 88 (2018) 488–496, https://doi.org/10.1016/j.jmbbm.2018.08.049.

[26] H. Wang, X.R. Zhang, H.C. Wang, J.K. Zhang, J. Li, C.S. Ruan, R. Zhu, K.L. Lin, Enhancing the osteogenic differentiation and rapid osseointegration of 3D printed Ti6Al4V implants via nano-topographic modification, J. Biomed. Nanotechnol. 14 (4) (2018) 707–715, https://doi.org/10.1166/jbn.2018.2551.

[27] H. Cai, Z.J. Liu, F. Wei, M. Yu, N.F. Xu, Z.H. Li, 3D Printing in spine surgery, Adv. Exp. Med. Biol. 1093 (2018) 345–359, https://doi.org/10.1007/978-981-13-1396-7_27.

[28] N.F. Xu, F. Wei, X.G. Liu, L. Jiang, H. Cai, Z.H. Li, M.A. Yu, F.L. Wu, Z.J. Liu, Reconstruction of the upper cervical spine using a personalized 3D-printed vertebral body in an adolescent with ewing sarcoma, Spine 41 (1) (2016) E50–E54, https://doi.org/10.1097/Brs.0000000000001179.

[29] F.B. Yu, J.H. Miao, X.Y. Liao, X.W. Wang, Y. Chen, D.Y. Chen, Evaluation of a new type of titanium mesh cage versus the traditional titanium mesh cage for single-level, anterior cervical corpectomy and fusion, Eur. Spine J. 22 (12) (2013) 2891–2896, https://doi.org/10.1007/s00586-013-2976-1.

[30] M.H. Mohammad-Shahi, V.S. Nikolaou, D. Giannitsios, J. Ouellet, P.F. Jarzem, The effect of angular mismatch between vertebral endplate and vertebral body replacement endplate on implant subsidence, J. Spinal Disord. Tech. 26 (5) (2013) 268–273, https://doi.org/10.1097/BSD.0b013e3182425eab.

[31] Z. Jing, T. Zhang, P. Xiu, H. Cai, Q. Wei, D. Fan, X. Lin, C. Song, Z. Liu, Functionalization of 3D-printed titanium alloy orthopedic implants: a literature review, Biomed. Mater. 15 (5) (2020), 052003, https://doi.org/10.1088/1748-605X/ab9078.

[32] H. Liu, W. Li, C. Liu, J. Tan, H. Wang, B. Hai, H. Cai, H.J. Leng, Z.J. Liu, C.L. Song, Incorporating simvastatin/poloxamer 407 hydrogel into 3D-printed porous Ti6Al4V scaffolds for the promotion of angiogenesis, osseointegration and bone ingrowth, Biofabrication 8 (4) (2016), https://doi.org/10.1088/1758-5090/8/4/045012.

[33] T. Zhang, Q.G. Wei, D.Y. Fan, X.G. Liu, W.S. Li, C.L. Song, Y. Tian, H. Cai, Y. F. Zheng, Z.J. Liu, Improved osseointegration with rhBMP-2 intraoperatively loaded in a specifically designed 3D-printed porous Ti6Al4V vertebral implant, Biomater. Sci-Uk 8 (5) (2020) 1279–1289, https://doi.org/10.1039/c9bm01655d.

[34] J. Lv, P. Xiu, J. Tan, Z.J. Jia, H. Cai, Z.J. Liu, Enhanced angiogenesis and osteogenesis in critical bone defects by the controlled release of BMP-2 and VEGF: implantation of electron beam melting-fabricated porous Ti6Al4V scaffolds incorporating growth factor-doped fibrin glue, Biomed. Mater. 10 (3) (2015), https://doi.org/10.1088/1748-6041/10/3/035013.

[35] T. Zhang, W.H. Zhou, Z.J. Jia, Q.G. Wei, D.Y. Fan, J.L. Yan, C. Yin, Y. Cheng, H. Cai, X.G. Liu, H. Zhou, X.J. Yang, Y.F. Zheng, Z.J. Liu, Polydopamine-assisted functionalization of heparin and vancomycin onto microarc-oxidized 3D printed porous Ti6Al4V for improved hemocompatibility, osteogenic and anti-infection potencies, Sci. Chn. Mater. 61 (4) (2018) 579–592, https://doi.org/10.1007/s40843-017-9208-x.

[36] M. Harries, M. Gore, Part I: chemotherapy for epithelial ovarian cancer - treatment at first diagnosis, Lancet Oncol. 3 (9) (2002) 529–536, https://doi.org/10.1016/S1470-2045(02)00846-X.

[37] S.A. Hundahl, Surgical quality in trials of adjuvant cancer therapy, J. Surg. Oncol. 80 (4) (2002) 177–180, https://doi.org/10.1002/jso.10123.

[38] M. Markman, Intraperitoneal chemotherapy, Crit. Rev. Oncol.-Hematol. 31 (3) (1999) 239–246, https://doi.org/10.1016/S1040-8428(99)00017-7.

[39] Y. Nagata, N. Araki, H. Kimura, K. Fujiwara, K. Okajima, T. Aoki, M. Mitsumori, K. Sasai, M. Hiraoka, T. Higuchi, S. Fujii, Neoadjuvant chemotherapy by transcatheter arterial infusion method for uterine cervical cancer, J. Vasc. Intervent. Radiol. 11 (3) (2000) 313–319, https://doi.org/10.1016/S1051-0443(07)61423-7.

[40] C.L. He, S.W. Kim, D.S. Lee, In situ gelling stimuli-sensitive block copolymer hydrogels for drug delivery, J. Contr. Release 127 (3) (2008) 189–207, https://doi.org/10.1016/j.jconrel.2008.01.005.

[41] L. Yu, J.D. Ding, Injectable hydrogels as unique biomedical materials, Chem. Soc. Rev. 37 (8) (2008) 1473–1481, https://doi.org/10.1039/b713009k.

[42] G.M. Zentner, R. Rathi, C. Shih, J.C. McRea, M.H. Seo, H. Oh, B.G. Rhee, J. Mestecky, Z. Moldoveanu, M. Morgan, S. Weitman, Biodegradable block copolymers for delivery of proteins and water-insoluble drugs, J. Contr. Release 72 (1–3) (2001) 203–215, https://doi.org/10.1016/S0168-3659(01)00276-0.

[43] Y.J. Kim, S. Choi, J.J. Koh, M. Lee, K.S. Ko, S.W. Kim, Controlled release of insulin from injectable biodegradable triblock copolymer, Pharm. Res. (N. Y.) 18 (4) (2001) 548–550, https://doi.org/10.1023/A:1011074915438.

[44] H.C. Ma, C.L. He, Y.L. Cheng, D.S. Li, Y.B. Gong, J.G. Liu, H.Y. Tian, X.S. Chen, PLK1shRNA and doxorubicin co-loaded thermosensitive PLGA-PEG-PLGA hydrogels for osteosarcoma treatment, Biomaterials 35 (30) (2014) 8723–8734, https://doi.org/10.1016/j.biomaterials.2014.06.045.

[45] P.S. Chan, J.W. Xian, Q.Q. Li, C.W. Chan, S.S.Y. Leung, K.K.W. To, Biodegradable thermosensitive PLGA-PEG-PLGA polymer for non-irritating and sustained ophthalmic drug delivery, AAPS J. 21 (4) (2019), https://doi.org/10.1208/s12248-019-0326-x.

[46] N. Chieng, M.T. Cicerone, Q. Zhong, M. Liu, M.J. Pikal, Characterization of dynamics in complex lyophilized formulations: II. Analysis of density variations in terms of glass dynamics and comparisons with global mobility, fast dynamics, and Positron Annihilation Lifetime Spectroscopy (PALS), Eur. J. Pharm. Biopharm. 85 (2) (2013) 197–206, https://doi.org/10.1016/j.ejpb.2013.03.036.

[47] M. Thommes, K. Kaneko, A.V. Neimark, J.P. Olivier, F. Rodriguez-Reinoso, J. Rouquerol, K.S.W. Sing, Physisorption of gases, with special reference to the evaluation of surface area and pore size distribution (IUPAC Technical Report), Pure Appl. Chem. 87 (9–10) (2015) 1051–1069, https://doi.org/10.1515/pac-2014-1117.

[48] S. Shahbazi, A. Zamanian, M. Pazouki, Y. Jafari, Introducing an attractive method for total biomimetic creation of a synthetic biodegradable bioactive bone scaffold based on statistical experimental design, Mater. Sci. Eng. C 86 (2018) 109–120, https://doi.org/10.1016/j.msec.2017.12.033.

[49] J.F.M. Ribeiro, S.M. Oliveira, J.L. Alves, A.J. Pedro, R.L. Reis, E.M. Fernandes, J. F. Mano, Structural monitoring and modeling of the mechanical deformation of three-dimensional printed poly(epsilon-caprolactone) scaffolds, Biofabrication 9 (2) (2017), 025015, https://doi.org/10.1088/1758-5090/aa698e.

[50] X. Zhang, M. Xu, L. Song, Y. Wei, Y. Lin, W. Liu, B.C. Heng, H. Peng, Y. Wang, X. Deng, Effects of compatibility of deproteinized antler cancellous bone with various bioactive factors on their osteogenic potential, Biomaterials 34 (36) (2013) 9103–9114, https://doi.org/10.1016/j.biomaterials.2013.08.024.

[51] N. Sarkar, S. Bose, Controlled delivery of curcumin and vitamin K2 from hydroxyapatite-coated titanium implant for enhanced in vitro chemoprevention, osteogenesis, and in vivo osseointegration, ACS Appl. Mater. Interfaces 12 (12) (2020) 13644–13656, https://doi.org/10.1021/acsami.9b22474.

[52] H. Xiao, R. Qi, S. Liu, X. Hu, T. Duan, Y. Zheng, Y. Huang, X. Jing, Biodegradable polymer - cisplatin(IV) conjugate as a pro-drug of cisplatin(II), Biomaterials 32 (30) (2011) 7732–7739, https://doi.org/10.1016/j.biomaterials.2011.06.072.

[53] Y. Ren, Y. Chen, X. Zheng, H. Wang, X. Kang, J. Tang, L. Qu, X. Shao, S. Wang, S. Li, G. Liu, L. Yang, Human amniotic epithelial cells ameliorate kidney damage in ischemia-reperfusion mouse model of acute kidney injury, Stem Cell Res. Ther. 11 (1) (2020) 410, https://doi.org/10.1186/s13287-020-01917-y.

[54] G. Carlsson, B. Gullberg, L. Hafström, Estimation of liver tumor volume using different formulas - an experimental study in rats, J. Canc. Res. Clin. Oncol. 105 (1) (1983) 20–23, https://doi.org/10.1007/bf00391826.

[55] W. Luo, J.Y. Wang, C.L. Liu, C. Huang, [Effect of electroacupuncture stimulation of "Feishu" (BL 13) on lung index, serum and lung IL-10 and TNF-alpha levels in mice with viral pneumonia], Zhen ci yan jiu = Acupuncture Research 39 (4) (2014) 293–297. https://pubmed.ncbi.nlm.nih.gov/25219125.

[56] Y. Li, W. Yang, X. Li, X. Zhang, C. Wang, X. Meng, Y. Pei, X. Fan, P. Lan, C. Wang, X. Li, Z. Guo, Improving osteointegration and osteogenesis of three-dimensional porous Ti6Al4V scaffolds by polydopamine-assisted biomimetic hydroxyapatite coating, ACS Appl. Mater. Interfaces 7 (10) (2015) 5715–5724, https://doi.org/10.1021/acsami.5b00331.

[57] P. Xiu, Z. Jia, J. Lv, C. Yin, Y. Cheng, K. Zhang, C. Song, H. Leng, Y. Zheng, H. Cai, Z. Liu, Tailored surface treatment of 3D printed porous Ti6Al4V by microarc oxidation for enhanced osseointegration via optimized bone in-growth patterns and interlocked bone/implant interface, ACS Appl. Mater. Interfaces 8 (28) (2016) 17964–17975, https://doi.org/10.1021/acsami.6b05893.

[58] N. Pabla, S. Huang, Q.S. Mi, R. Daniel, Z. Dong, ATR-Chk2 signaling in p53 activation and DNA damage response during cisplatin-induced apoptosis, J. Biol. Chem. 283 (10) (2008) 6572–6583, https://doi.org/10.1074/jbc.M707568200.

[59] W.P. Roos, B. Kaina, DNA damage-induced cell death: from specific DNA lesions to the DNA damage response and apoptosis, Canc. Lett. 332 (2) (2013) 237–248, https://doi.org/10.1016/j.canlet.2012.01.007.

[60] D. Woods, J.J. Turchi, Chemotherapy induced DNA damage response: convergence of drugs and pathways, Canc. Biol. Ther. 14 (5) (2013) 379–389, https://doi.org/10.4161/cbt.23761.

[61] D. Wang, S.J. Lippard, Cellular processing of platinum anticancer drugs, Nat. Rev. Drug Discov. 4 (4) (2005) 307–320, https://doi.org/10.1038/nrd1691.

[62] Y.W. Jung, S.J. Lippard, Multiple states of stalled T7 RNA polymerase at DNA lesions generated by platinum anticancer agents, J. Biol. Chem. 278 (52) (2003) 52084–52092, https://doi.org/10.1074/jbc.M310120200.

[63] S. Zhu, N. Pabla, C. Tang, L. He, Z. Dong, DNA damage response in cisplatin-induced nephrotoxicity, Arch. Toxicol. 89 (12) (2015) 2197–2205, https://doi.org/10.1007/s00204-015-1633-3.

[64] G. Dai, L. Yu, J. Yang, K. Xia, Z. Zhang, G. Liu, T. Gao, W. Guo, The synergistic antitumor effect of cinobufagin and cisplatin in human osteosarcoma cell line in vitro and in vivo, Oncotarget 8 (49) (2017) 85150–85168, https://doi.org/10.18632/oncotarget.19554.

[65] M.A. Lopez-Heredia, E. Goyenvalle, E. Aguado, P. Pilet, C. Leroux, M. Dorget, P. Weiss, P. Layrolle, Bone growth in rapid prototyped porous titanium implants, J. Biomed. Mater. Res. 85 (3) (2008) 664–673, https://doi.org/10.1002/jbm.a.31468.

[66] K.C. Stine, E.C. Wahl, L.C. Liu, R.A. Skinner, J. VanderSchilden, R.C. Bunn, C. O. Montgomery, L.J. Suva, J. Aronson, D.L. Becton, R.W. Nicholas, C. J. Swearingen, C.K. Lumpkin, Cisplatin inhibits bone healing during distraction osteogenesis, J. Orthop. Res. 32 (3) (2014) 464–470, https://doi.org/10.1002/jor.22527.